VOL. IX - N.º 1 - 1987 ISSN 0100-7386

REVISTA BRASILEIRA DE CIÊNCIAS MECÂNICAS

PUBLICAÇÃO DA ABCM
ASSOCIAÇÃO BRASILEIRA DE CIÊNCIAS MECÂNICAS

A Revista Brasileira de Ciências Mecânicas é uma publicação técnico-científica, da Associação Brasileira de Ciências Mecânicas. Destina-se a divulgar trabalhos significativos de pesquisa científica e/ou tecnológica nas áreas de Engenharia Civil, Mecânica, Metalurgia, Naval, Nuclear e Química e também em Física e Matemática Aplicada. Pequenas comunicações que apresentem resultados interessantes obtidos de teorias e técnicas bem conhecidas serão publicadas sob o título de Notas Técnicas.

Os Trabalhos submetidos devem ser inéditos, isto é, não devem ter sido publicados anteriormente em periódicos de circulação nacional ou internacional. Excetuam-se em alguns casos publicações em anais e congressos. A apreciação do trabalho levará em conta a originalidade, a contribuição à ciência e/ou tecnologia, a clareza de exposição, a propriedade do tema e a apresentação. A aceitação final é da responsabilidade dos Editores e do Conselho Editorial.

Os artigos devem ser escritos em português, ou espanhol ou em inglês, datilografados, acompanhados dos desenhos em papel vegetal, em tamanho reduzido que permita ainda a redução para as dimensões da Revista e enviados para o Editor Executivo no endereço abaixo.

Editor Executivo da RBCM
Secretaria da ABCM
PUC/RJ - ITUC
Rua Marquês de São Vicente, 225 - Gávea
22453 - Rio de Janeiro, RJ - Brasil

A composição datilográfica será processada pela própria secretaria da RBCM de acordo com as normas existentes.

The Revista Brasileira de Ciências Mecânicas (Brazilian Journal of Mechanical Sciences) is a technical-scientific publication, sponsored by the Brazilian Association of Mechanical Sciences. It is intended as a vehicle for the publication of Civil, Mechanical, Metallurgical, Naval, Nuclear and Chemical Engineering as well as in the areas of Physics and Applied Mathematics. Short communications presenting interesting results obtained from well-known theories and techniques will be published under heading of the Technical Notes.

Manuscripts for submission must contain unpublished material, i.e., material that has not yet been published in any national or international journal. Exception can be made in some cases of papers published in annals or proceedings of conferences. The decision on acceptance of papers will take into consideration their originality, contribution to science and/or technology. The Editors and the Editorial Committee are responsible for the final approval.

The papers must be written in Portuguese, Spanish or English, typed and with graphics done on transparent white drawing paper in reduced size in such a way as to permit further reduction to the dimensions of the Journal, and sent to the Executive Editor at the following address.

Executive Editor of RBCM
Secretary of ABCM
PUC/RJ - ITUC
Rua Marquês de São Vicente, 225 - Gávea
22453 - Rio de Janeiro, RJ - Brazil

The final typing will be done by the secretary of RBCM according to the journal norms.

REVISTA
BRASILEIRA DE
CIÊNCIAS
MECÂNICAS

Vol. IX nº 1 – Fev. 1987

SILGRAF ARTES GRÁFICAS LTDA.
TEL.: 263-5685 – 233-0017

A REVISTA BRASILEIRA DE CIÊNCIAS MECÂNICAS É PUBLICADA COM O APOIO

DO CNPq E FINEP
COMPANHIA VALE DO RIO DOCE
IBM DO BRASIL

COBEM·87

IX CONGRESSO BRASILEIRO DE ENGENHARIA MECÂNICA
9th BRAZILIAN CONGRESS OF MECHANICAL ENGINEERING

7 - 11 DE DEZEMBRO DE 1987

FLORIANÓPOLIS - SANTA CATARINA - BRASIL

ÁREAS COBERTAS

. PROJETO MECÂNICO
. PROCESSOS DE FABRICAÇÃO
. INSTRUMENTAÇÃO, AUTOMAÇÃO E METROLOGIA
. VIBRAÇÕES E ACÚSTICA
. MECÂNICA DOS SÓLIDOS E ESTRUTURAL
. MÉTODOS NUMÉRICOS
. TERMODINÂMICA
. TRANSFERÊNCIA DE CALOR E MASSA
. MECÂNICA DOS FLUIDOS
. SISTEMAS E EQUIPAMENTOS TÉRMICOS E HIDRÁULICOS

SCOPE

. MECHANICAL DESIGN
. MANUFACTURING PROCESSES
. AUTOMATION, INSTRUMENTATION, AND METROLOGY
. ACOUSTICS AND VIBRATION
. SOLID AND STRUCTURAL MECHANICS
. NUMERICAL METHODS
. THERMODYNAMICS
. HEAT AND MASS TRANSFER
. FLUID MECHANICS
. THERMAL AND HYDRAULIC SYSTEMS, AND EQUIPMENTS

PROMOÇÃO
(PROMOTED BY)

UFSC
1987 25 ANOS

DEPARTAMENTO DE ENGENHARIA MECÂNICA
UNIVERSIDADE FEDERAL DE SANTA CATARINA

ABCM

ASSOCIAÇÃO BRASILEIRA DE CIÊNCIAS MECÂNICAS

INFORMAÇÕES GERAIS
(GENERAL INFORMATION)

LIMITE PARA ENTREGA DOS RESUMOS — 20/03/87
(ABSTRACT DUE — MAR. 20, 1987)
LIMITE PARA ENTREGA DOS TRABALHOS — 15/06/87
(FULL-LENGTH PAPER DUE — JUN. 15, 1987)
ENDEREÇO P/ CORRESPONDÊNCIA *(MAILING ADRESS)*

COBEM/87
DEPT. ENGENHARIA MECÂNICA - UFSC
CX. P. 476 — FLORIANÓPOLIS, SC
88049 — BRASIL

TELEFONE: (0482) 339397 - 33-9225
TELEX: (0482) - 240 - UFSCBR

THE COUPLED PROBLEM OF THE OPERATING TEMPERATURES AND ELASTOHYDRODYNAMIC LUBRICATION (EHL) OF ROLLING CONTACT BEARINGS

V. A. Schwarz
Department of Mechanical Engineering
Escola Federal de Engenharia de Itajubá, MG

B. R. Reason
School of Mechanical Engineering
Cranfield Institut of Technology
Cranfield, Bedford – England

ABSTRACT

A theoretical and experimental investigation on temperature distribution (steady state) and heat generation in bath lubricated radial roller bearings has been carried out. A brief description of the test rig, bearings and lubricants employed is given. A technique is presented for the theoretical prediction of the bearing heat generation, temperature distribution (including roller temperature) and oil film thicknesses in the elasto-hydrodynamic contacts between the most heavily loaded roller and the raceways. Some typical results are presented; a good correlation being obtained between the theoretical and experimental data.

NOMENCLATURE

A	Surface area (m^2)
C	Dynamic load rating (N)
C_i	Combined variable coefficients in eqs.(20-26); $i = 1,2,3,...$
$C_{i,o}$	Constants in eq.(13)
D_m	Bearing pitch diameter (m)
D_r	Roller diameter (m)
E'	Reduced elastic modulus (N/m^2)

$$\frac{1}{E'} = \frac{1}{E_r} + \frac{1}{E_t}$$

$E_{r,t}$ Roller and raceways (tracks) materials elastic moduli (N/m^2)
F_r Radial load applied to the bearing (N)
$f_{i,o}$ Friction torque coefficients
h EHL oil film thickness (m)
$h_{i,o}$ EHL oil film thickness at the roller/inner, outer raceway contact (m)
H_c Thermal contact conductance (W/m^2K)
H_g Heat generation per unit time (W)
k Thermal conductivity (W/m ^{o}C)
$k_{1,2}$ Constants in eq.(14)
ℓ Effective length of a bearing roller (m)
M Total bearing friction torque (N·m)
M_0 Viscous friction torque (N·m)
M_1 Load dependent torque (N·m)
n Shaft speed (rpm)
Q Heat transfer rate (W)
Q_{i-j} Heat transfer rate from node i to j (i,j = 1,2,...) in eqs.(20-26) (W)
R' Equivalent radius (m)

$$\left(\frac{1}{R'}\right)_{i,o} = \frac{1}{R_r} \pm \frac{\cos\alpha}{R_{i,o}}$$

$R_{i,o}$ Inner, outer raceway radius (m)
R_r Roller radius $R_r = D_r/2$ (m)
s Ratio between the roller and the pitch diameter of the bearing $s = D_r/D_m$
t_o Oil temperature (^{o}C)
$t_{1,2}$ Temperatures of the surfaces 1 and 2, in eq.(1); temperatures of nodes 1 and 2, in eqs.(20 and 23) (^{o}C)
$t_{i,o}$ Temperatures of the inner, outer raceway (^{o}C)
$t_{i,j}$ Temperatures of nodes i and j in eqs.(20-26) i,j = 1,2,3,... (^{o}C)
t_t Raceway (track) temperature (^{o}C)
t_r Roller temperature (^{o}C)
u Combined surface velocity (m/s)

$$u = \frac{1}{2}\left(u_{i,o} + u_r\right)$$

$u_{i,o,r}$ Surface velocities of the inner or outer raceway, and roller (m/s)
W' Load per unit length (N/m)

Z	Number of rollers (N/m)
Z_c	Number of rollers that support the load
α	Contact angle of a taper roller bearing
β	Pressure viscosity coefficient (m^2/N)
ν	Kinematic viscosity of the lubricant (mm^2/s)
η_o	Dynamic viscosity of the lubricant at the entry EHL contact ($N \cdot s/m^2$)

INTRODUCTION

The accurate calculation or measurement of the operating temperatures of a rolling contact bearing and its lubricant is essential for the prediction not only of the bearing and lubricant service life, but also of any mechanical failure that could arise from differential thermal expansions among the bearing components (rings and rolling elements), shaft and housing.

It is well known, from many references, such as [1,2] that the bearing wear and service life is highly dependent on the elastohydrodynamic lubrication (EHL) oil film thicknesses "h" established between the most heavily loaded roller (or ball) and the raceways.

These oil film thicknesses are direct functions of the lubricant viscosity "ν" and by implication of the operating temperatures, as ν varies dramatically with temperature. On the other hand, as will be shown in this paper, the operating temperatures of the bearing rolling elements and raceways are dependent on h. Furthermore, the operating temperatures are obviously dependent on the bearing heat generation (which is a direct function of the lubricant viscosity) and the heat dissipation capibilities of the assembly.

Therefore, this interdependence among the above factors gives rise to a extremely complex problem. A literature survey shows that previous attempts for the solution of the theoretical problem gave unsatisfactory results. Schwartz [3] calculated temperature that were considerably higher than his experimental values. On the other hand, his calculated bearing heat generation was lower than that found experimentally by him. These two lack of correlation between his theoretical and experimental results are in "apparent" contradiction, as a lower heat generated should imply in lower operating temperatures, or vice-versa (this will be discussed in the "Conclusions").

The principal reason for the innacurate theoretical results has been an inadequate estimate of the heat dissipation potential of the housing, shaft and any cooling effect. Other reasons, equally important, are the innacurate evaluation of the following factors:

- percentage of heat (relative to the total heat generated by the bearing) generated in the various sources of friction in the component parts of the bearing;
- heat imput to the bearing from external sources;
- heat transfer coefficients.

An assessment with solid basis of the above factors can only be obtained from extensive experimental results, complemented by a sound theoretical analysis. These are the objectives of this work.

THE TEST RIG AND EXPERIMENTAL RESULTS

A full description of the test rig, instrumentation, and experimental results is given in [4,5,6], therefore only a brief outline will be presented here.

Figure 1 shows the general arrangement and indicates two bearing options on the central section. In a first stage of the experimental work, two identical taper roller bearing "B" were mounted back-to-back (as shown above the centre-line) in the central housing, whilst two identical cylindrical roller bearings "A" were fitted onto each end of the test-shaft. In a second stage of experiments, the bearings B were replaced by a single self-aligning double row spherical roller bearing "C", as shown below the centre--line in Figure 1.

The test bearings were as follows:

- Bearings "A": RHP MRJ 1 ¾"
- Bearings "B": TIMKEN 4595/4536
- Bearings "C": SKF 22310 CJ/C3 W33

The bearing housing to the left is a conventional one (bolted down to the bedplate). On the other hand, both the central and the right housings consist of cylindrical sleeves supported on hydrostatic bearings, such that the friction torques from the corresponding roller bearings can be simultaneously measured by two torque measurement systems. One of these torque systems, which are composed by load-cells and torque-arms, may be seen in cross-section BB.

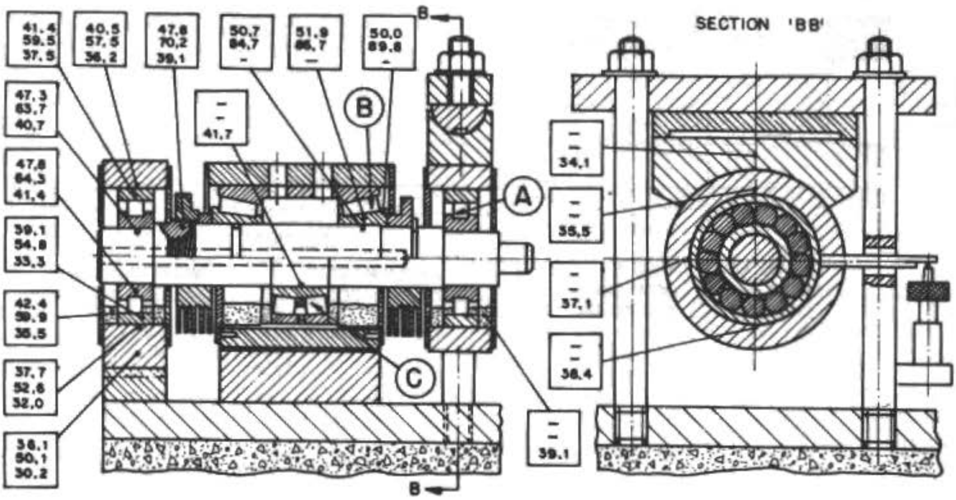

Figure 1. General arrangement of the test module, the steady state temperatures measured in three different tests

The radial load applied to the right roller bearing "A" is measured by two transducers (strain-gauge bridges mounted on the twin pillars bolted down the bedplate).

For purposes of assessing the spatial temperature distribution throughout the roller bearings, housings and shaft an array of Chromel/Constantan thermocouples is used, each couple being located at a specific nodal point represented by the small black circles in Figures 1 and 2.

Thermocouples and transducers signals are transmitted to a "Fluke 2200B" sixty-channel data-logger for capture and signal conditioning. The accuracy of ±0.1°C between 0-1000°C specified by the makers was confirmed on laboratory calibration.

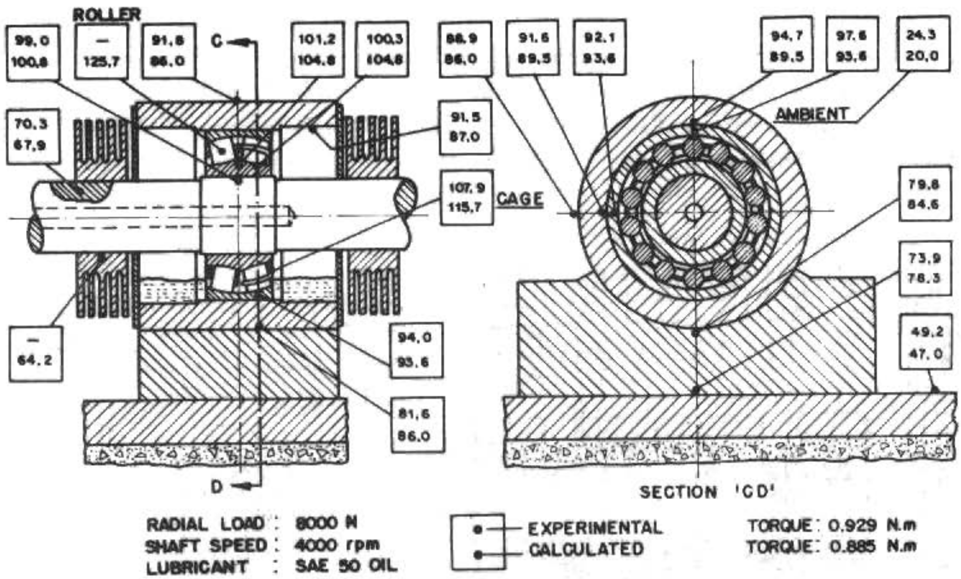

Figure 2. Temperature distribution (°C) bearing SKF 22310 CJ/C3 W33

The inner rings and shaft thermocouple wires (taken out through the hollow shaft) were connected to a high-quality silver/ /silvergraphite slip ring unit, and from this to the data-logger.

Figure 1 also shows, in each "square" linked to the corresponding nodal point, the three steady-state temperature values measured at three different tests. The operating conditions of the end bearings A were maintained constant during the three tests, as follows:

- Shaft speed: 1000 rpm ,
- Radial load: 1500 N ,
- Bath lubrication: SAE 30 oil.

However, different bearings, or different axial loading conditions, were used for the central bearing unit, as indicated in Table 1.

Table 1. (To be analysed together with Figure 1)

Bearing type(s) and preloading conditions for the central bearing	Temperatures °C	Torque (N·m)	
a) Twin taper roller bearings "B"/light axial preload	a)	0.33	measured at the rear cylindrical roller bearing "A"
b) Twin taper roller bearings "B"/preload: 3KN	b)	0.29	
c) Single self-aligning spherical roller bearing	c)	0.35	

The two most important observations from the three different set of temperature values shown in Figure 1 are:

1) The significant influence of the central bearing temperatures on those of the left end bearing. Even though the duty conditions of this left end bearing were kept constant during the three different tests, its steady-state temperatures were appreciably different for each of the three tests.

2) The fundamental effect of the heat dissipation potential of each bearing assembly. The temperature values, measured at corresponding points of the left bearing A and the central bearing C, were approximately the same, even though the heat generated by bearing C was almost twice that of the bearing A.

Therefore, the important conclusion (obvious but generally disregarded in the literature) is that "any attempt to calculate the operating temperature of a bearing assembly will be successful only if both its heat dissipation capability and the influence of any adjacent device can be evaluated with sufficient accuracy".

THEORETICAL ANALYSIS

As already mentioned, the spacial temperature distribution of a rolling contact bearing assembly can only be calculated as a result of a thermal balance between the bearing heat generation (plus any external heat from seals and adjacent devices) and the heat dissipation capability of the assembly (including any cooling device).

Thus, in the theoretical analysis, all the heat sources and heat transfer modes, listed below, must be considered simultaneously:

a) conductive heat transfer from the housing base to the foundations;

b) heat conduction from the bearing outer ring to the housing;

c) heat conduction from the bearing inner ring to the shaft;

d) axial heat conduction along the shaft, including heat inputs from outside the bearing system proper;

e) conductive heat transfer at the EHL contacts between the rollers and the raceways;

f) convective heat transfer from the outer surface of the housing to the environment;

g) radiation of heat from the housing outer surface to the surroundings;

h) convective heat transfer from the rotating shaft to the surrounding fluids;

i) convective heat transfer from the bearing components to the surrounding fluid (s) inside the housing;

j) heat generated (friction power losses) between pairs of surfaces in relative motion, i.e.: rolling elements/raceways, rolling elements/cage, roller ends/ring shoulders, cage/ring (s). Additionally, the heat generation from viscous churning may be a major heat source and must be considered.

Basic Equations

Heat transfer equations. The basic heat transfer equations may be found in [5,6 and 7]. Only those equations and heat transfer coefficients not commonly given in text books will be discussed here.

Relative to the itens b and c, above, it is important to emphasize that the thermal conductivity of roller bearing steels is equal to about 30 $W/m^{o}C$, whilst that of standard shaft and housing steels is equal to 50 $W/m^{o}C$, approximately.

In considering the itens a, b, and c, the conduction of heat between two contiguous bodies, through the common contacting surface, may be calculated by the equation:

$$Q_S = H_C A(t_1 - t_2) \qquad (1)$$

The thermal contact conductance, H_c in equation (1), is an extremely complex function of the following factors: combined surface roughness of the pair of contacting surfaces, roundness of two fitted cylindrical surfaces (e.g. shaft/bearing inner rings), waviness and flatness of two flat surfaces in contact, hardness of the contacting materials, load under which the two surface are pressed against each other, physico/chemical layers occuring in or on the interfacial asperities. Based on the theoretical and experimental results from refs.[8 and 9], and on the experimental data obtained with the authors test ring (Figure 1), the following values of H_c were adopted in this theoretical analysis:

- H_c = 20000 W/m^2K for the shrinkfit mounting of the bearing inner ring on the shaft;
- H_c = 15000-20000 for the outer ring/housing fit, and for the housing base/bedplate metallic contact;
- H_c = 450 W/m^2K for the bedplate/concrete block contacting surfaces.

Relative to the heat transfer mode especified in item e, it has been demonstrated by Cheng ref.[10] and other scientists that conduction across the oil film is the chief heat transfer mechanism in an EHL contact, convection being negligible. The rate of heat conduction from a loaded roller to the inner and outer raceways of the bearing can be calculated by the following equation:

$$Q_0 = K_0 \frac{A}{h} (t_r - t_t) \qquad (2)$$

The thermal conductivity K_0 of an SAE 30 oil varies with temperature approximately as follows:

$$K_0 = 0.130 - 0.00007t \qquad (3)$$

This equation may also be applied to the other two test oils (SAE 20W and SAE 50) with negligible errors.

The heat flow area in eq.(2) is given by the product of the roller effective length ℓ in the EHL contact zone, the Hertzian flat width b, and the number Z_c of rollers that support the load within the Stribeck zone, viz:

$$A = \ell \cdot b \cdot Z_C \tag{4}$$

The Hertzian band width b, derived from refs.[11 and 12], may be expressed as:

$$b = 6.691 \times 10^{-6} \left(\frac{4.08\ F_r\ R'}{\ell \cdot Z \cdot \cos\alpha} \right) \tag{5}$$

It is known [12,13,14] that the load supported by each roller within the Stribeck zone varies with the angular position of the roller, and is proportional to the bearing dimensions and applied load. Furthermore, the number of rollers that support the load is also dependent upon the housing configuration and on the thichness of its walls [14]. However, to obtain an averaging effect for purposes of heat transfer calculations, it was assumed that the radial load applied to the bearing is evenly distributed amongst the Z_C loaded rollers and that $Z_C = Z/4$. These assumptions and the use of eq.(5) are recommended only for bearings under pure radial loads in the range $0.06C < F_r < 0.12C$, where C is the basic dynamic load rating of the bearing ref.[15]. For bearings under axial or combined loads see ref.[6].

Regarding to the item f one must keep in mind that the convective heat dissipation from the housing outer surface is dependent upon the air flow around the housing; this air flow being, in many applications, a direct function of the rotational speed, shape, and proportions of the shaft or machine elements mounted on the shaft.

The heat transfer by forced convection between the moving parts of the bearing and the adjacent fluids inside the housing (item i) represents extremely complex mechanisms. The corresponding equations, derived from refs.[16 and 17], are given in ref.[6].

EHL oil film thickness equation. By analysing their experimental data obtained with the traditional disc-machines, Dyson et al. ref.[18] and Wilson ref.[19] showed that the EHL oil film thickness "h", calculated by using the Dowson and Higginson's "isothermal theory" equation ref.[13] correlate well with those experimental data (provided $h < 1\ \mu m$).

A literature survey indicates that experimental values of h in rolling contact bearings are usually less than 0.7 μm, examples of this being given in refs. [20,21].

Therefore, it was decided to develop a simplified EHL oil film thickness equation for roller bearings, following Bolton's guidelines ref.[2] and based on Cheng's isothermal formula ref.[22], written as follows:

$$\frac{h}{R'} = 1.987 \left[\frac{\eta_0 \; \beta u}{R'}\right]^{0.74} \left[\frac{W'}{E'R'}\right]^{-0.11} \tag{6}$$

For mineral oils, according to references [2] and [23], the product of the dynamic viscosity "η_0" and the pressure viscosity coefficient "β" may be conveniently expressed solely as a function of the kinematic viscosity, viz:

$$\eta_0 \beta = 8.5 \times 10^{-12} \; \nu^{1.18} \tag{7}$$

Substituting eq.(7) into eq.(6) yields:

$$h_{i,o} = 12.763 \left[\frac{R'_{i,o}}{D_m}\right] D_m \; \nu^{0.873} \left[\frac{u}{R'}\right]_{i,o} \left[\frac{W'}{E'R'_{i,o}}\right]^{-0.11} \tag{8}$$

where the subscripts "i,o" refer to parameters calculated for a roller/inner or outer raceway contact.

From the Notation it can be demonstrated that

$$R'_{i,o} = \left[\frac{1 \pm s}{2\cos\alpha}\right] s \cdot D_m \tag{9}$$

The roller motion in the Stribeck zone of a roller bearing may be assumed as being essentially epicyclic if the bearing pitchline speed is not excessively high (i.e. < 15 m/s), and if the applied load is greater than 0.1C, in order to avoid roller skidding. For these conditions, therefore, the following relationship, demonstrated in ref.[12], is realistic, viz:

$$u_i = u_o = u_r = \frac{0.5\pi}{60} \, n(1 - s^2) D_m \tag{10}$$

Dividing eq.(10) by eq.(9), gives:

$$\left[\frac{u}{R'}\right]_{i,o} = \frac{\pi}{60} \left[\frac{1 \pm s}{s}\right] n \cdot \cos\alpha \tag{11}$$

The load parameter W' (load per unit length) for radial roller bearings of conventional clearances is given in references [12 and 13], as follows:

$$W' = \frac{4.08\ F_r}{Z \cdot \ell \cdot \cos\alpha} \tag{12}$$

Substituting eqs. (9, 11 and 12) into eq. (8) and knowing that for steels $E' = 2.275\ (10)^{11}\ N/m^2$, yields:

$$h_{i,o} = C_{i,o} \cdot D_m \cdot n^{0.74} \cdot \nu^{0.873} \cdot F_r^{-0.11} \tag{13}$$

where the constants $C_{i,o}$ calculated for the three test bearings are given as follows:

COEF.	BEARING TYPE		
	MRJ 1 3/4"	4595/4536	22310 CJ/C3 W33
C_i	3.052×10^{-9}	3.239×10^{-9}	3.375×10^{-9}
C_o	3.512×10^{-9}	3.598×10^{-9}	3.878×10^{-9}

Note: For taper roller bearings under axial or combined loads see ref. [6].

The lubricant Kinematic viscosity ν of the test oils (SAE 20W, 30, and 50), according to laboratory tests, varies with temperature as follows:

$$\log \log(\nu + 0.6) = K_1 \cdot \log(t_o + 273.15) + K_2 \tag{14}$$

where the constants $K_{1,2}$ are given as follows:

OIL	K_1	K_2
SAE 20W	-3.6338	9.3356
SAE 30	-3.5022	9.0432
SAE 50	-3.3924	8.8435

For substituting eq.(14) into eq.(13) it is of fundamental importance to remember that the oil temperature "t_o" must be considered as a mean between the temperatures of the roller and the inner (or outer) raceway. This is based on the well established EHL principles given in ref.[13], viz: "In considering the effect of viscosity upon film thickness it is the viscosity of the oil at the temperature of the specimens which is the controlling factor and that the temperature of the oil bath has no influence whatever, except insofar as it may affect the temperature of the contacting bodies. Furthermore, h is governed by the lubricant properties (η_o,β) in the entry region of the EHL contact."

Thus, the prediction of the oil film thickness between the rolling elements and raceways is only possible if the temperatures of these bearing components can be measured or predicted with some certainty. COnversely the calculation of the roller and raceways temperatures requires the calculation of these oil film thickness; see eq.(2).

Heat generation equations. The heat generated per unit time (friction power losses) in a rolling contact bearing is given by:

$$H_g = \frac{\pi\, n\, M}{30} \tag{15}$$

where the total bearing torque may be calculated by:

$$M = M_1 + M_0 \tag{16}$$

$$M_1 = f_1\, F_r\, D_m \tag{17}$$

$$M_0 = f_0 (\nu n)^{2/3}\, D_m^3\, 10^{-1} \tag{18}$$

The coefficients "f_1" and "f_0" are given in refs.[12 and 15], for all types of rolling contact bearings. For the test-bearings the following values were adopted:

	BEARING DESIGNATION		
	MRJ 1 3/4"	4595/4536	22310 CJ/C3
f_1	0.000375	0.0005	0.0005
f_0	3.0	4.0	6.0

Based on the experimental and theoretical results from refs. [6, 24 and 25], the following percentage of the total heat generated was estimated at each bearing heat source, viz:

a) Roller/inner raceway	20-40%
b) Roller/outer raceway	20-40%
c) Roller/cage pockets	8-12%
d) Cage/land riding ring	8-12%
e) Roller ends/guide flange	0.1-0.8%
f) Viscous churning of lubricant	8-40%

Note: The predominant influence on the above distribution of generated heat is the lubricant quantity in the bearing. The maximum percentage value (40%) for the item "f", which corresponds to a 50% immersion of the lowest roller [ref.6], results in the minimum percentages for the other heat sources. Conversely, the minimum percentage value (8%), which corresponds t_o a minimum lubricant quantity, results in the maximum percentages for the other heat sources.

Temperature Prediction Technique

The "Heat Balance Method", as described by Welty [26] was employed as the foundation to the programme for calculating the operating temperatures within a bearing assembly (as already explained, the bearing heat generation and EHL oil film thickness must be calculated simultaneously with the temperatures, requiring the use of a computer).

Basically the method involves the thermal equilibrium conditions within a structure and consits of equating the total heat influx to a given point or "node" (including any thermal energy generated at the node) to the total heat efflux from this node to the adjacent ones.

An initial step involves the selection of a set of elements or nodes (points or surfaces whose temperatures are to be calculated) throughout the structure. The accuracy of the analysis depend on the number of nodes and their position. Figure 2 shows the nodes selected in the central bearing assembly (together with the measured and predicted nodal temperatures for a specific duty conditions).

As a second step the heat balance method is applied to each node, all modes of heat transfer being considered. For illustrative purposes consider Figure 2 with the following arbitrary selection of nodal points i and corresponding tempearatures t_i:

Node 1 - Bearing roller	t_1
Node 2 - Outer raceway	t_2
Node 3 - Outer surface of the bearing outer ring	t_3
Node 4 - Bearing cage	t_4

Applying the heat balance method to node "2" gives:

$$Q_{1-2} + 0.1\,H_g = Q_{2-3} + Q_{2-4} \tag{19}$$

The heat transfer rate Q_{1-2} from Node 1 to Node 2 in eq.(19) corresponds specifically to the eq.(2), i.e. conductive heat transfer through oil film. Similarly, Q_{2-3} illustrates radial heat conduction from Node 2 to Node 3, whilst Q_{2-4} represents heat transfer by forced convection from Node 2 to Node 4 (see refs. 6, 16 and 17). The percentage of heat generated "$0.1\,H_g$" at Node 2, in eq.(19) correspond to the item b - previous section; the concepts given by Burton [27] being considered. Burton suggested that the heat generated by two surfaces in relative motion is equally dissipated between the two surfaces at the contact.

Substitution of eqs.(3-5, 13 and 14) into eq.(2) yields:

$$Q_{1-2} = C_1 (t_1 - t_2) \tag{20}$$

Obviously, the coefficient C_1 is a complex non-linear function of the proper temperatures t_1 and t_2. Similarly, Q_{2-3} and Q_{2-4} can be represented in a simplified manner, as follows:

$$Q_{2-3} = C_2 (t_2 - t_3) \tag{21}$$

$$Q_{2-4} = C_3 (t_2 - t_4) \tag{22}$$

Substituting eqs.(20, 21 and 22) into eq.(19) gives:

$$C_1 (t_1 - t_2) + 0.1\,H_g - C_2 (t_2 - t_3) - C_3 (t_2 - t_4) = 0 \tag{23}$$

This final equation (23) is, therefore, the result of applying the heat balance method to Node 2 and illustrates a typical nodal equation.

As a second illustrative example of obtainning a typical nodal equation, consider Figure 2 with the following nodal points i and corresponding temperatures t_i:

Node 5 - Shaft portion at the bearing seating t_5
Node 6 - Shaft portion at the cooling fins seating t_6
Node 7 - Main body of the fins system t_7

Applying the heat balance method to Node 6 gives:

$$Q_6 + Q_{5-6} - Q_{6-7} = 0 \quad (24)$$

"Q_6" represents axial heat conduction along the shaft from the two end bearings to Node 6. In any practical situation this could be calculated by applying an ordinary heat conduction equation,provided the shaft temperatures near the end bearings (or machine device) could be evaluated with some degree of accuracy. In the present analysis, however, Q_6 was considered as a thermal energy generated at Node 6 and equal to a given percentage C_4 of the heat generated in the bearing in studdy, viz:

$$Q_6 = C_4 \; H_g \quad (25)$$

From the discussions at the end of Section 2, the inclusion of Q in eq.(24) is paramount for the accuracy of the theoretical analysis.

"Q_{5-6}" represents axial heat conduction from Node 5 to Node 6, whilst "Q_{6-7}" stands for radial heat conduction from Node 6 to Node 7.

Representing the ordinary heat conduction equations Q_{5-6} and Q_{6-7} in a simplified manner, and substituting in eq.(24) gives:

$$C_4 H_g + C_5 (t_5 - t_6) - C_6 (t_6 - t_7) = 0 \quad (26)$$

Eq.(26) illustrates, therefore, a second typical nodal equation, i.e. similar to eq.(23).

It is obvious from the foregoing that similar equations will pertain for each of the remaining selected nodal points. Thus a system of "N" non-linear equations is obtained, (N = number of nodes selected within the bearing assembly). Using the vector notation

"$\mathfrak{t}$" to indicate the vector of unknows (t_1, t_2, ... t_N), this system of non-linear equation may be written as follows:

$$f_i(\mathfrak{t}) \equiv f_i(t_1, t_2, \ldots, t_N) = 0 \; ; \qquad i = 1, 2, 3, \ldots, N \qquad (27)$$

The third and final step of the process is to obtain the solution of the system of equations (27), which will then represent the predicted nodal temperatures, This may be accomplished by using the computer program given in [6], such that other important factors are simultaneously calculated, e.g., bearing torque, heat generation, and EHL oil film thicknesses.

DISCUSSION OF THE RESULTS

Theoretical and Experimental Temperature and Torque Correlation

Figure 2 shows both the measured and the theoretically predicted temperatures for the central bearing assembly. Experimental and calculated magnitudes of bearing friction torque are also included. The degree of correlation between the measured and predicted temperatures and torque is noteworthy.

Temperature correlations for non-rotating points above and below the bearing horizontal centre line. The theoretical temperature distribution within the bearing outer ring and the housing was assumed to produce isotherms of symmetrical configuration relative to the bearing centre, e.g. circumferences or ellipses. However, as shown in Figures 1 and 2, points within the upper half of the housing and bearing outer ring were at higher temperatures than those of corresponding points at the lower half. This explains the following correlation between the experimental and calculated temperatures, over all the wide range of tests:

a) The better correlation is observed for points at the level of the bearing horizontal axis, calculated temperatures being 1-2% higher than the experimental values.

b) Calculated temperatures resulted to be 2-5% lower than the experimental values for points within the upper half of the housing and outer ring of the bearing; the opposite correlation being observed for points within the lower half.

The reason for the "asymmetrical" temperature distribution is the greater heat dissipation rates from the lower halves of the left and central housings (upper half of the right housing - Figure 1). This aspect is fully discussed in refs. [4, 5 and 6].

Roller temperature. An important aspect of the theoretical results is that the predicted roller temperatures were some 10-20% higher than those of the inner ring, as shown in Figures 2, 3 and 4. Since roller temperatures were not measured in the test rig, current literature was searched for some substantiation of this result. Experimental confirmation of this prediction was found in the results by Norlander and Stackling [28] who measured rolling element temperatures some 18% higher than those measured at the inner ring of a deep groove ball beering.

Inner raceway and cage temperatures. The calculated temperature of the inner raceway and the cage were about 2-3% and 5-7% higher than the experimental values, respectively (see Fig.2).

Friction torque correlation. In general, calculated friction torque was some 2-4% lower than the measured values, as shown, for example, in Figure 2.

Note: From the foregoing discussion it has been shown that the predicted temperatures were slightly higher than the experimental values, whilst, on the other hand, calculated torques were slightly lower than the measured ones. The conclusion is, therefore, that the "heat dissipation potential" of the bearing assembly was slightly underestimated in the theoretical analysis. This will be further discussed in the following section.

Variation of bearing temperatures and torque with speed. Figures 3 and 4 show the variation of calculated temperatures and torques with speed and with load. The profile of the theoretical curves lie very close to those of the experimental curves given in [6], except for loads lighter than about 2-3 KN; the calculated torques and temperatures being higher than the experimental values for these light loads.

Predicted oil film thicknesses between the rollers and the inner raceway are thinner than those between the rollers and the outer raceway. This is due, not only to the better degree of conformity and larger equivalent radius for the outer raceway contact, but also because the outer raceway temperature is lower than that of the inner raceway (see Figs. 3 and 4).

Effect of speed on EHL oil film thickness. Figure 3 show the variation of calculated EHL oil film thicknesses, "$h_{i,o}$", with shaft speed. It can be seen that $h_{i,o}$ increased rapidly with speed (up to about 500-700 rpm) and then decreased gradually with speed, for speeds above that value. This is due to the significant decrease of both the lubricant viscosity and pressure-viscosity coefficient as temperature increased with speed.

Such variation of $h_{i;o}$ with speed is in close agreement with the experimental results from [20].

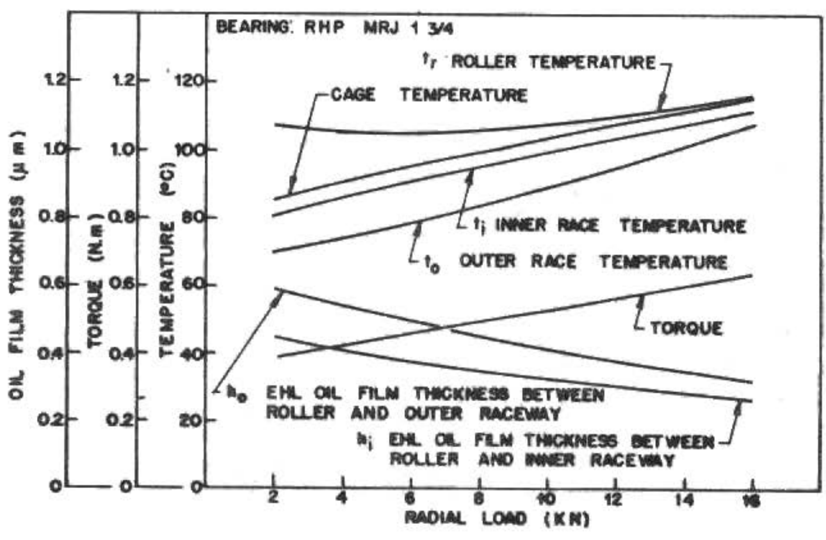

Figure 4. The effect of load on calculated temperatures, torque and oil film thicknesses. Shaft speed: 4000 rpm. Lubricant: SAE 30 oil (half immersion on lowest roller)

Effect of lubricant quantity and viscosity grade. Figure 5 shows the significant effect of oil quantity (immersion level of the lowest roller) on the measured torques and temperatures of the spherical roller bearing.

Similarly, the use of a heavier oil means higher torques and temperatures for the bearing [6].

EHL Oil Film Thickness Results

Calculated EHL oil film thicknesses of the roller/inner (and outer) raceway contacts are plotted (together with bearing temperatures and torques) in Figures 3 and 4, for various speed or load conditions.

For the reasons pointed out in Section "EHL oil film thickness equation", a mean between the roller and raceway temperatures was adopted when calculating lubricant viscosity and the corresponding EHL oil film thickness. It is to be inferred that the higher roller temperature (relative to the raceway temperature) has, therefore, a significant effect upon the EHL oil film thickness.

Computer calculated oil film thicknesses are in good agreement with the experimental results obtained by Pemberton and Cameron [20] and by Wilson [21].

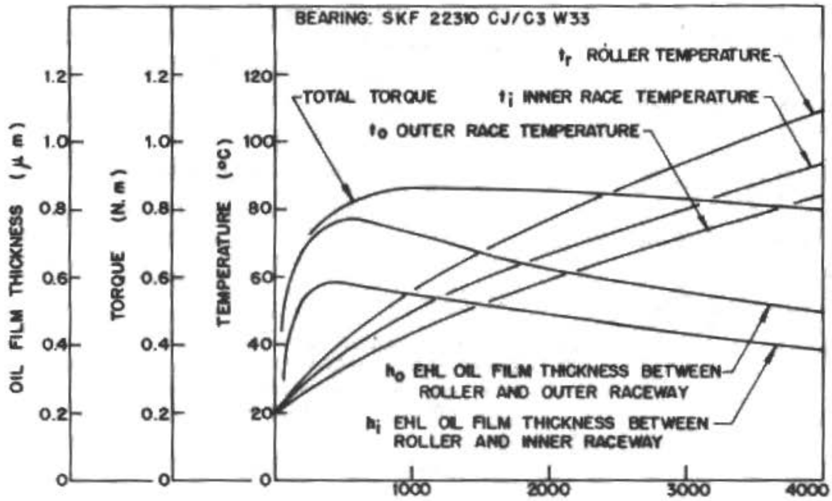

Figure 3. The effect of speed on calculated temperatures, torque and oil film thicknesses, radial load: 8000 N. Lubricant: SAE 30 oil (half immersion of lowest roller)

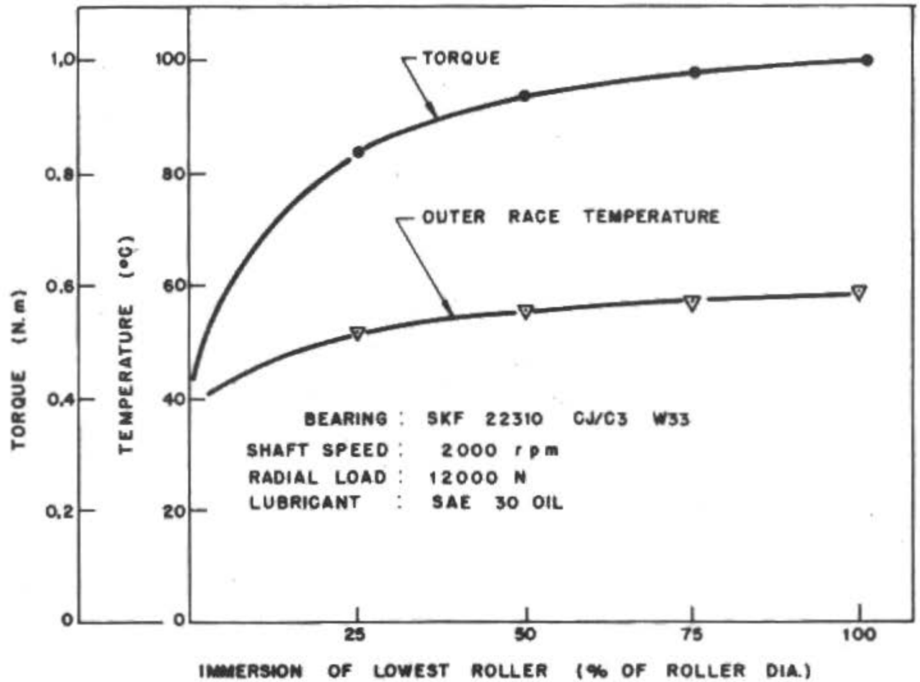

Figure 5. Measured effect of oil quantity on bearing torque and temperature

Effect of load on EHL oil film thickness. Figure 4 shows the variation of oil film thicknesses, temperatures and torque with applied load. It can be seen that oil film thicknesses decreased by about 20% for a load increase of 100%. This dependence on load is slightly in excess of that found experimentally by Crook, as reported in [13]. Oil film thicknesses decreases with load not only due to the load parameter in eq.(13) but also due to the effect of load on the operating temperatures (Figure 4) and, consequently, on the lubricant viscosity, since, as may be seen from eq.(14), the kinematic viscosity ν decreases drammatically with temperature.

Thermal Balance

Figure 6 shows both "Heat Generation" and "Heat Dissipation" curves plotted against the outer race temperature for the spherical roller bearing SKF 22310 CJ/C3 W33. A corresponding ordinate for the bearing friction torque is also included.

Three bearing "Heat Generation" curves are plotted, corresponding to the choice of SAE 20W, SAE 30, or SAE 50 oils. Since the heat generated by the bearing is a function of the lubricant viscosity (which is an inverse function of the temperature) heat generation decreases with temperature. This effect is clearly shown by the three "Heat Generation" curves.

Three "Heat Dissipation" curves are plotted; the "Total Heat Dissipation" corresponding to the sum of the "Heat Dissipation through the Housing" and the "Heat Dissipation through the Shaft/ /Fins".

The point of interception of each of the three "Heat Generation" curves and the "Total Heat Dissipation" curve represents the thermal equilibrium condition and indicates both the bearing outer race temperature and the friction torque for the specified operating condition (load, speed and lubricant).

It is immediately obvious that the choice of the thinner oil would result in a lower operating temperature and reduced power loss in the bearing unit. It is to be appreciated that a lower operating temperature implies increased oil change periods, since oil oxidation rate is lowered.

Figure 6 also shows the importance of an accurate assessment of the heat dissipation potential of the assembly. If this is underestimated (for example, if the "Heat Dissipation through the Shaft/Fins" if neglected), there is an apparent anomaly in that the predicted temperature is higher than the experimental one, whilst the calculated friction torque is less than the corresponding measured value. This phenomenon is readily explained, however, on the basis of the rapid decrease of the lubricant viscosity with temperature. If the heat dissipation is underestimated in the programme, the predicted bearing temperature will, obviously be higher, giving a lower operating viscosity. Since the friction torque equation used in the programme itself contains a viscosity term, the result will be a predicted friction torque lower than the measured value.

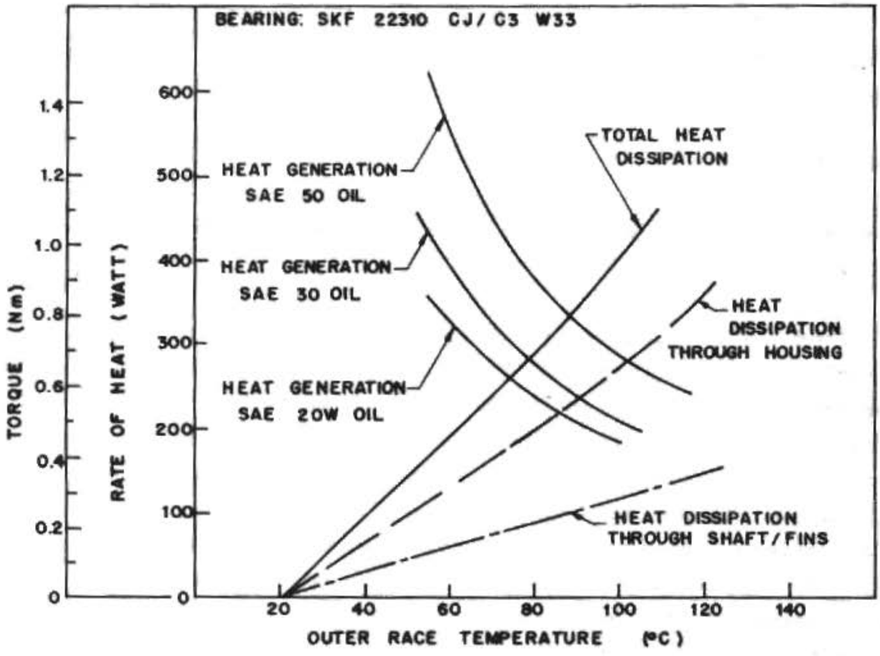

Figure 6. Thermal balance, shaft speed: 4000 rpm, radial load: 4000 N, oil level: half immersion of lowest roller

As already discussed in Section 1, apparently, this effect was experienced by Schwartz [3], the experimental and theoretical findings reported in his paper giving a similar "contradiction" in the two parameters.

The effect was demonstrated, somewhat dramatically for the authors, during early development work on the programme. In normal running, after thermal equilibrium is reached, an appreciable amount of heat is conducted out of the bearing from the housing base to the bedplate. This was, initially, underestimated in the earlier programmes, the resultant temperatures being, in certain cases, almost 50% higher than those experimentally measured, whilst the calculated torques from the programme were, unexpectedly, less than those measured on test.

The problem was finally resolved when thermocouples were placed at the base of the housings (see Figure 1). These gave a true picture of the extent of the conduction heat transfer. It is to be inferred, therefore, in the light of this, that close attention to foundation conduction is highly relevant when assying thermal problems in bolted-down bearing housings.

CONCLUSIONS

Influence of Adjacent Bearings and Heat Dissipation Potential of the Assembly

From the discussions in the previous section, it is clearly shown that both the operating temperatures and friction torque of any bearing assembly are hightly dependent on both the temperatures of adjacent bearings (or machine devices) and the heat dissipation potential of the assembly (housing/foundations, shaft and any specific cooling device). These effects must, therefore, be given careful consideration in any theoretical attempt to predict the temperature distribuition and heat generation within a bearing assembly, if a good correlation between theoretical and experimental results is hoped to be obtained.

In the authors opinion, inaccurate estimates of the heat dissipation and/or failure to consider the effect of the operating temperatures of adjacent bearings clearly explain some of the comments (In the "Discussions" of selected papers in the literature) regarding too high or too low friction torque (or heat generation) for a given bearing type and size.

Effect of Lubricant Quantity and Viscosity

As discussed in previously, increased lubricant quantity significantly increases bearing friction torque and operating temperatures. On the other hand, it is evident from eq.(13) that the EHL oil film thickness decreases with temperature (temperature/ /viscosity chanracteristics of the lubricant).

It can be concluded, therefore, that the common practice of specifying rolling contact bearings with the lowest rolling element half immersed in the oil bath, may not be further recommended. Less lubricant quantity would result in less heat generation within the bearing, lower operating temperatures (and thereby increased relubrication intervals) and, possibly, thicker oil films in the EHL contacts (thus increased bearing service life) provided lubricant starvation is unlike to manifest - see [20 and 29]. Additionally, another advantage of reducing the lubricant quantity would be the consequent reduction in roller skidding [30].

Similarly, the use of a less viscous lubricant would result in less power loss from the bearing and lower operating temperatures, as discussed in previously. However, EHL oil film thickness would also be reduced, the lubricant selection being made therefore from a compromise between these parameters.

Further Conclusions on EHL Oil Film Thickness

By employing the simplified EHL oil film thickness formula, i.e. eq.(13), the following conclusions were obtained:

a) Substantially thick EHL oil films may be established between the rollers and raceways of a roller bearing, for a shaft speed as low as 50 rpm.

b) Typically, "$h_{i,o}$" (EHL oil film thickness between roller and inner or outer raceway) increases rapidly with speed (for $n < 500$ rpm), remaining approximately constant with speed (for $500 < n < 1000$) and decreasing gradually with speed (for $n > 1000$ rpm).

c) Somewhat surprisingly, "$h_{i,o}$" calculated for n = 100 rpm were larger than "$h_{i,o}$" for n = 3000 rpm.

d) "$h_{i,o}$" decreases, somewhat significantly with load, for bath lubricant roller bearings.

e) Usually, "h_i" is about 20% lower than "h_o". This has been confirmed by Wilson [21].

Note: These conclusions "a", "b" and "c" above have been experimentally confirmed by Pemberton and Cameron [20].

ACKNOWLEDGEMENTS

Many thanks are due to Brian Moffitt and Mike Devonshire of the Cranfield SME Instrumentation Laboratory for their invaluable assistance. In addition, V.A. Schwarz gratefully acknowledges the sponsorship from Escola Federal de Engenharia de Itajubá and CAPES, Brasil, under which it was possible to carry out this study.

REFERENCES

[1] Tallian, T.E. — On competing failure modes in rolling contact. ASLE Trans., 10 : 418-439, 1967.

[2] Bolton, W.K. — Elastohydrodynamics in practice. In: International Symposium on "Rolling Contact Fatigue: Performance Testing of Lubricants," The Institute of Petroleum, London, Pub. Heyden and Son Ltd., London, 1976. p.17-25.

[3] Schwartz, J.I. — Friction-induced heating in axially loaded ball bearings. Trans. ASME, Journal of Lubrication Technology, January 1976, p.105-112.

[4] Reason, B.R. and Schwarz, V.A. — A thermal prediction technique for extending in-service life of roller bearing assembiles. NBS Special Publication 640, MFPG, National Bureau of Standards, Washington D.C., USA, 1981. p.295-325.

[5] Schwarz, V.A. and Reason, B.R. — Mitigation of thermal hazards in rolling contact bearings through correlated computer analysis. AGARD Conference Proceedings nº 323 - Problems in Bearings and Lubrication, Ottawa, Canada, 1982. p.9-16, NTIS.

[6] Schwarz, V.A. — Experimental and analytical studies on temperature distributions in bath lubricated radial roller

bearing assemblies. Ph.D. Thesis, Cranfield Institute of Technology, 1982.

[7] Wong, H.Y. – Heat transfer for engineers. Longman, N.Y., 1977.

[8] Brunot, A.W. and Buckland, F.F. – Thermal contact resistance of laminated and machined joints. ASME Trans., 1949, p.253-267.

[9] Veziroglu, T.N. – Correlation of thermal contact conductance experimental results. Progr. Astron. Aero. 20, Academic Press Inc., New York, 1967, p.879-907.

[10] Cheng, H.S. – Calculation of elastohydrodynamic film thickness in high-speed rolling and sliding contacts. Mechanical Technology Incorporated, Report 67TR24, 1967.

[11] Cheng, H.S. – A numerical solution of the elastohydrodynamic film thickness in an elliptical contact. Journal of Lubrication Technology, ASME Trans., January 1970, p.155-162.

[12] Harris, T.A. – Roller bearing analysis. John Wiley, New York, 1966.

[13] Dowson, D. and Higginson, G.R. – Elastohydrodynamic lubrication. SI Edition. Pergamon Press, 1977.

[14] Munnich, H. et al. – The effect of elastic deformation on load distribution in rolling bearings. Ball Bearing Journal 155, SKF.

[15] SKF General Catalogue 3200 E, 1981.

[16] Bjorklund, I.S. and Kays, W.M. – Heat transfer between concentric rotating cylinders. ASME Trans., Journal of Heat Transfer, August 1959. p.175-186.

[17] Sparrow, E.M. and Gregg, J.L. – Heat transfer from a rotating disk to fluids of any Prandtl number. Journal of Heat Transfer, 81 : 249-251, 1959.

[18] Dyson, A: et al. – The measurement of oil-film thickness in elastohydrodynamic contacts. Proc. Inst. Mech. Engrs., v.180, Pt. 3B, p.119-134, 1965-66.

[19] WIlson, A.R. – An experimental thermal correction for predicted oil-film thicknesses in elastohydrodynamic contacts. Thermal Effects in Tribology, Paper VII (i), I.Mech. E., 1980, p.179-190.

[20] Pemberton, J.C. and Cameron, A. – An optical study of the lubrication of a 65mm cylindrical roller bearing. Journal of Lubrication Technology, ASME Trans., v.101, p.327-337, 1979.

[21] Wilson, A.R. – The relative thickness of grease and oil-film in rolling bearings. Proc. Inst. Mech. Engrs., v.193, p.185-192, 1979.

[22] Cheng, H.S. – A numerical solution of the elastohydrodynamic film thickness in an elliptical contact. Journal of Lubrication Technology, ASME Trans., January 1970, p.155-162.

[23] Bamberger, E.N. et al. – Life adjustment factors for ball and roller bearings. An engineering design guide. ASME, 1971.

[24] Garnell, P. – Further investigations of the mechanics of roller bearings. Proc. Inst. Mech. Engrs., v.181, Pt.1, no.16, p.339-348, 1966-67.

[25] Astridge, D.G. and Smith, C.F. – Heat generation in high-speed cylindrical roller bearings. Elastohydrodynamic Lubrication 1972, Inst. Mech. Engrs., London, p.83-94.

[26] Welty, J.R. – Engineering heat transfer. John Wiley & Sons, New York, 1974, p.38-65.

[27] Burton, R.A. and Staph, H.E. – Thermaly activated seizure of angular contact bearings. ASLE Trans., v.10, 1967, p.408-417.

[28] Norlander, G. and Stackling, H. – A new way to measure temperature. Ball Bearing Journal 172, SKF.

[29] Wedeven, L., Evans, D. and Cameron, A. – Optical analysis of ball bearing starvation. Trans. ASME/ASLE, Series F, v.93, no.3, July 1971, p.349-363.

[30] Boness, R.J. – The effect of oil supply on cage and roller motion in a lubricated roller bearing. Journal of Lubrication Technology, ASME Trans., v.92, no.1, January 1970, p.39-53.

A COMPUTER PACKAGE FOR THE MODELLING AND ANALYSIS OF MULTIBODY SYSTEMS

José Eduardo Zindel Deboni
IPEN – Instituto de Pesquisas Energéticas e Nucleares
CNEN/SP

ABSTRACT

The use of computer programs in system dynamic analysis is very common. Frequency responses, vibration modes and time simulations can be calculated by the computer, if one has a mathematical model of the system. These kind of analysis is useful in many fields of mechanical engineering, such as rotor dynamics, vehicle technology and machine design. THis work presents some programs developed for microcomputers that simplify these studies. The engineer creates a model by connecting rigid bodies, springs, dampers and external excitations. The model equations must be supplied by linear second order equations, put in a matrix form. The results of the analysis are stored for post-processing or plotting in a graphic terminal. The user can make changes in model equations and model parameters, and verify how these changes affect the system dynamic behavior. In the second part of this work, a small rotor with elastic bearings is modelled and analysed. The bearing parametes are estimated by a simple procedure. The method is to rationally variate the parameters, until a good agreement is found between the calculated transfer function, and an experimental one.

RESUMO

O uso de programas de computador na análise dinâmica de sistemas é algo bastante comum. Respostas em frequências, modos de vibração e simulações podem ser realizados facilmente se tivermos um modelo matemático do sistema em questão. Estes tipos de análises são de extrema importância em diversos campos da engenharia mecânica, tais como: dinâmica de rotores, tecnologia de veículos e projeto de máquinas. O presente trabalho apresenta alguns programas desenvolvidos para microcomputadores que simplificam estes estudos. O engenheiro cria o modelo unindo corpos rígidos, molas, amortecedores e excitações externa. As equações do modelo devem ser descritas por equações diferenciais lineares de segunda ordem colocadas na forma matricial. Os resultados da análise são armazenados para pós-processamento ou traçado em um terminal gráfico. O usuário pode fazer alterações nas equações ou nos parâmetros e verificar como estas alterações afetam o comportamento dinâmico do sistema. Na segunda parte do trabalho, um pequeno rotor com mancais elásticos é modelado e estudado. Os parâmetros do mancal são estimados através de um procedimento simplificado. O método consiste em variar racionalmente os parâmetros até que se tenha uma função de transferência calculada que se aproxime bem da função experimental.

INTRODUCTION

The use of computer programs to solve some system dynamics problems is very common. The engineer can estimate the behavior of a system if he has a mathematical description of that system. So we can understand modelling as the representation of a real system for the analysis of some of its characteristics. Among many techniques of modelling, the multibody approach is very close to mechanical systems with applications to rotor dynamics, vehicle technology, robotics and machine design.

The objective of this paper is to present a group of programs developed to the analysis of multibody systems in a 16 bits microcomputer. There are some excelent general purpose programs for analysing system dynamics, a good review of them can be found in [1]. These programs provide an easy way to the user to build and simulate the systems. The cost of the microcomputers is motivating its use in technological field and although restricted to simple models one can find applications such as simulations, verification of confort in vehicles, optimization of parameters to increase stability, evaluate frequency responses or vibration modes.

Some important requirements have to be remembered when developing a software of this kind. First of all the operation must be interactive so the user can control of the execution as he like, in this way the interface between man and machine must be efficient to an expert as to a beginner user. The programs must provide an easy and fast way for changing the model parameter values and verifying its influence in the system dynamic behavior. Standard outputs are necessary to interchange data between other programs, and for post processing too. Graphical output is an other important feature that must be provided; and of course, accurancy and computational efficiency must be taken into account.

THE MATHEMATICAL MODEL

Extensive literature exists on linear systems [3], and there are also many well established numerical algorithms on this broad field of system dynamics. So as a first step in the development of the package only linear systems will be considered. A well known representation of a mechanical model is the second order differential equation, that can be put in a matrix form, such as:

$$RM*\ddot{X} + P*\dot{X} + Q*X = H \quad (1)$$

where RM,P and Q are known as mass, damping and spring matrices respectively; abd H is the external forces vector. The degrees of freedom and its derivatives with respect to time are represented by the $X, \dot{X}$ and $\ddot{X}$ vectors.

Other restrictions had to be imposed such as time independence and real constant coefficients. The model in this form is used for frequency response calculations where complex external forces (2) and frequency dependent parameters are allowed.

$$H = Hr + j*Hi \quad (2)$$

From the matrix equation (1) a state-space representation can be developed, if the RM matrix is positive definite. The state space representation is put in an also well known matrix equation (3) where the matrices are built as indicated in (4) and (5). This representation will be used for eigenvalue calculation and for time simulation.

$$\dot{Y} = A*Y + B*U \quad (3)$$

where

$$Y^T = X^T \,\vdots\, \dot{X}^T \qquad B = 0 \,\vdots\, RM^{\ T} \qquad U = 0 \,\vdots\, Hr^T \quad (4)$$

$$A = \left[\begin{array}{c|c} 0 & I \\ \hline -RM^{-1}*P & -RM^{-1}*Q \end{array}\right] \quad (5)$$

The model equations must be delivered by the user, it can be formulated by a Lagrangean approach or by applying the Newton's and Euler's laws to the system. THis may be a very difficult and time consumming task. A new solution to the problem of developing the model equations that apper in the last decade are some general purpose software for generating the symbolic equations of motion [1]. In our applications the NEWEUL program [2] has been used with very good results. This program can generate the model equation and the user has only to provide a description of the system, its inertia tensors, masses, forces and moments as functions of the geometric properties and the degrees of freedom. The studied case will show a simple use of this package.

GENERAL DESCRIPTION OF THE SOFTWARE

The high level language used for the development of the packege was Pascal, in order to improve maintenance and portability to the software. The system of programs were designed to be structured and modular so the first step was to define some standards for the input and output. Then the algorithms were selected and tested, and only afterwards the package was built. The numerical methods were selected mainly because of its generality; the QR algorithm is used to evaluate both real and complex eigenvalues and eigenvectors of the system matrices; to integrate the differential equations a 4th order Runge-Kutta method is used. When a matrix needs to be inverted a Gauss-Jordan Inversion procedure is called. An important part of the programs is a formula interpreter that was designed to evaluate the equations of motion without the need of re-compilation. This interpreter has the same structure of the Pascal language itself and can solve the commun mathematical functions such as sin, cos, exp, etc...

The following figure shows the general interaction between some concepts involved in the program.

In the Figure 1 we can see that the real system can be modelled with the help of the NEWEUL program, that delivers the equations of motion, whitch can be edited to create an input data file with the model equations in a format suitable to the ADS program. On the other hand measurements and experimentation can be performed in the system and the results will be the numerical values for the parameters of the model or other experimental results. Those experimental results will, in the future, feed an identification scheme to provide the parameters too.

After the model equations and the model parameters have been developed, the main program can be executed, and the user can interactively perform the analysis. Today we can divide the analysis into four classes: Frequency calcations, Matrix calculation, Eigenvalues and Time simulation. Now we will describe in a little more detail each one of these.

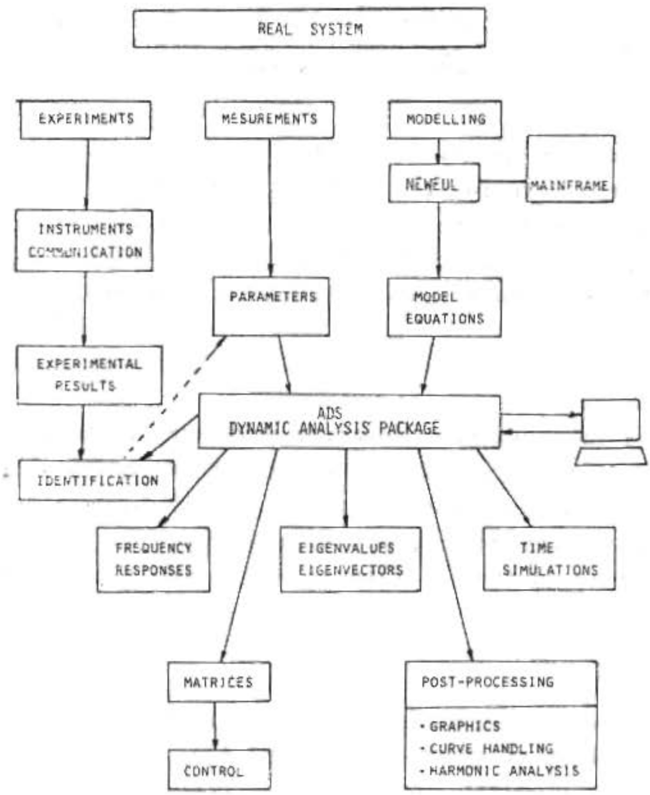

Figure 1. Block diagram of the program package

Frequency Calculations

Based on the n second order differential equations, the program can construct a system of n complex linear equations on the unknown degrees of freedom as shown in (6). The complex system of order n is transformed into a real system of order 2n and then solved, as (7).

$$((Q - W2*RM) + j*W*P)*(Xr + j*Xi) = Hr + j*Hi \tag{6}$$

were W is the frequency [Rad/s]. The subscripts r and i indicate the real and complex components.

$$\begin{Bmatrix} Xr \\ Xi \end{Bmatrix} = \left[\begin{array}{c|c} Q-W2*RM & -W\ P \\ \hline W*P & Q-W2*RM \end{array}\right] * \begin{Bmatrix} Hr \\ Hi \end{Bmatrix} \qquad (7)$$

choosing suitably Hr and Hi, and variating W in a given range it can calculate the transfer function of a system, a forced harmonic response or an unbalance response. As the equations are solved for each frequency, the matrices RM, P, Q and H can have W as a parameter. The results are stored in a magnetic media for post processing.

Matrix Calculation

All the matrices that describe numerically the system can be outputed, and listed. The future use for these matrices will be some control design programs, that will use the modern control theory. Once a state description of the system is known, one can minimize a linear quadratic criteria and estimate the feedback matrix, for example.

Eigenvalues

Estimation of eigenvalues is made by estimating the real and complex eigenvalues of the matrix A, and also the eigenvectors. Then they are sorted, from the lower to the upper complex eigenvalue, or eigenfrequency. This calculation can be performed for a single set of parameters and the modes of vibration are then normalized and listed; or one can variate any of the model parameters and verify its influence in the eigenvalues. This last type of analysis is called sensivity analysis and shows the variation of natural frequencies and stability with the system parameters; in this case the outputs can also be stored.

Time Simulation

The system (4) can be integrated with respect to time for a given set of initial values and using some excitation. The program provides some standard excitations such as random noise, ramp, pulse, step or sin functions. The integration scheme is very much time consumming. A general purpose integration program that will deal with non linear models as well as with linear ones is now under development.

Post Processing

Graphics is the most important post processor. The program can draw graphics on the computer graphic terminal and then transfer them to a pen plotter, or to a dot-printer for hardcoping. Linear and Logarithimic scales are avaliable.

Another very usefull post processing is the curve handler. With this program one can operate numerically the stored results of the main program. The curves can be interpolated, multiplied, added, and function such as sin, cos, exp can be performed in the data to estimate coupling forces, other points of the rigid bodies motion, or functions can be integrated or derivated in the frequency domain.

CASE STUDIED: ROTOR WITH ELASTIC BEARINGS

A small air driven rotor was taken as an example, to demostrate the use of the programs. Figure 2 shows the system which consists of an aluminium rotor of about 400 mm long, with ball bearings at both ends to allow free turnig, driven by a small air turbine that can run up to 6000 rpm. At the ends there is a rigid shaft conecting a copper disk to a flexible spring. The copper disk oscilates in a constant magnetic field created by coils, in order to deliver some damping to the system. This aparatus was built at GEPROM [4] or educational propouses in rotor dynamics.

The ADS program will be used to estimate the flexibility and damping parameters of the bearings. The method variates this parameters until a good agreement between experimental and theoretical transfer functions of the system is found.

The first step is to develop a mathematical model for the real system. As we will be interested in the low frequency range (below 3000 rpm) the rotor can be assumed rigid, and a model of a rigid rotor with flexible and damped bearings seems to be a good representation for this system. Let's supose also that the bearings have radial simetry, ie the spring and damping constants for both axis X, Y are equal.

Figure 3 describes the mathematical model, and the symbols to be used. This figure also provide the input data to the modelling program NEWEUL [2] that will develop the model equations. To describe the model to the program is necessary to answer some

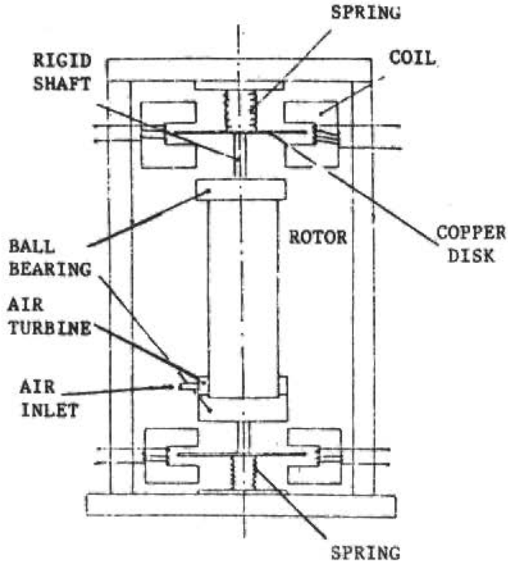

Figure 2. Rotor system

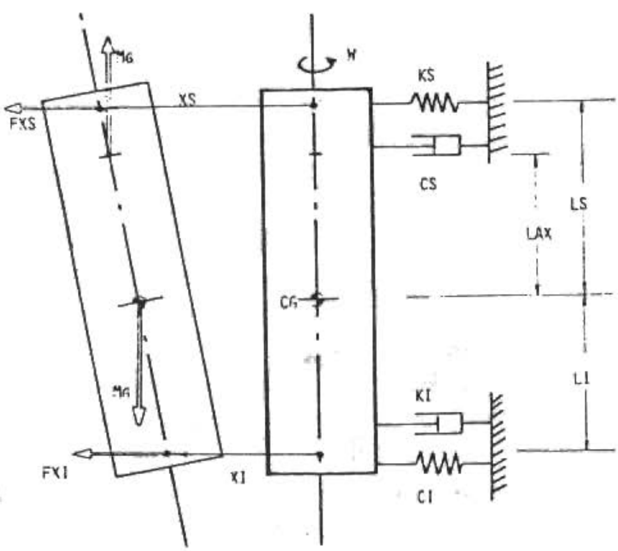

Figure 3. Multibody model representation

questions as the numbers of bodies, numbers of degrees of freedom, the names for the position vector, the mass and inertia tensor as well as the forces and moments that are applied to the bodies. After that, a list of the model matrices as shown in Figure 4 for the mass matrix, is outputed.

```
RM(1,1)=LI**2*LM1**2*M+J*LM1**2
RM(1,2)=LS*LI*LM1**2*M-J*LM1**2
RM(1,3)=0.
RM(1,4)=0.
RM(2,2)=LS**2*LM1**2*M+J*LM1**2
RM(2,3)=0.
RM(2,4)=0.
RM(3,3)=LI**2*LM1**2*M+J*LM1**2
RM(3,4)=LS*LI*LM1**2*M-J*LM1**2
RM(4,4)=LS**2*LM1**2*M+J*LM1**2
with LM1=1.0/(LI+LS)
```

Figure 4. Mass matrix output listing

Using a text editor these equations can be easily edited to create a data file for the ADS programs. Another data file must be breated with the numerical values for the model parameters, this file will contain a list, such as in Figure 5.

```
M=6.8
J=0.1854
JP=0.005736
LI=0.294
LS=0.275
LAX=0.37
FXS=1.0
W=0.0
G=9.806
```

Figure 5. Parameter data file list

The analysis program will now be used to identify the spring and damping parameters (KS,KI,CS,CI). An experimental test was carried out to suply the transfer function. The test consists in estimating on an spectrum analyser, with the FFT algorithm, the transfer function between the signal of a load cell connected to a hammer that excites the rotor, and an accelerometer, mounted on the upper bearing. The experimental set up is represented in Figure 6.

The calculation used 512 data points with a cut off frequency of 25Hz. Figure 6 also exibits the resulting curve, where we can find the two natural frequencies corresponding to the modes of vibration; the lower one is at 5.5Hz and the upper one on 9.7Hz.

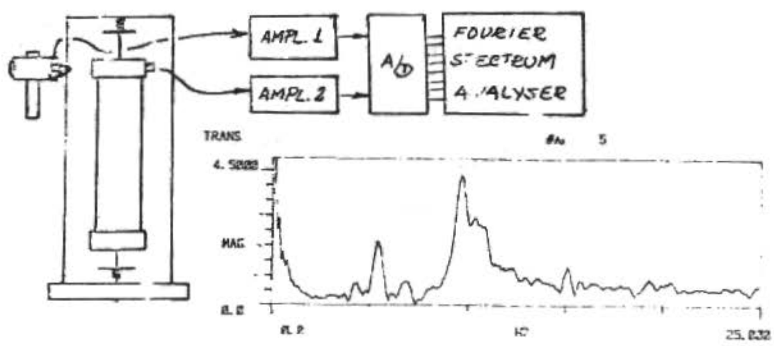

Figure 6. Experimental transfer function

It is well known that the spring constants greatly influence the eigenfrequencies; so we can use this fact in the identification. It is possible with the programs to variate the spring constants and calculate the eigenvalues of the model until the imaginary part of them matches the two frequencies. As there are two spring constant this variation is not so easy and can even lead to a non unique solution. A simple static test was made to relate the two spring constants (KS and KI), and reduce the number of parameters to be identified. The test is to measure the displacements at the two bearings and find a point in the rotor were the application of a force would produce the same displacement in the two springs; at that moment the ratio between the distance of that point and the bearings is equal to the ratio of the spring constants, as shown in Figure 7. It was found that the KS/KI ration is approximatly equal to 1.45. Now we can study the effect of the KI (KS=1.45*KI) in the eigenvalues. Figure 8 shows the result of this variation. It also shows that the value of 3.4*10^-3 leads to a very good approximation to the correct values for the natural frequencies.

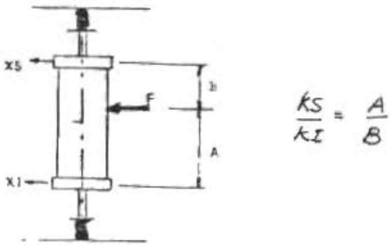

Figure 7. Static determination of the KS KI ratio

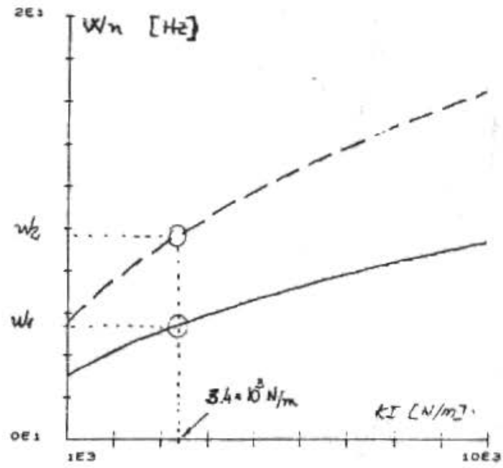

Figure 8. Variation of KI x Wn (the value of Ki selected so that the eigenfrequencies are matched)

The next step in identification is to select the damping coefficients. Assuming for simplicity that they are equal:

$$C = CS = CI$$

we can calculate the theoretical transfer functions XS/FXS for some values of C and compare it with the experimental one. The transfer function of the díisplacement is easily calculated from the second order equation, and it can be transformed into an acceleration function by multiplying the gain values by W^2. Figure 9 shows the displacement transfer function and the comparison to the experimental curve. The selected value of C=7 N/(m/s) is the one that give the best agreement among the curves.

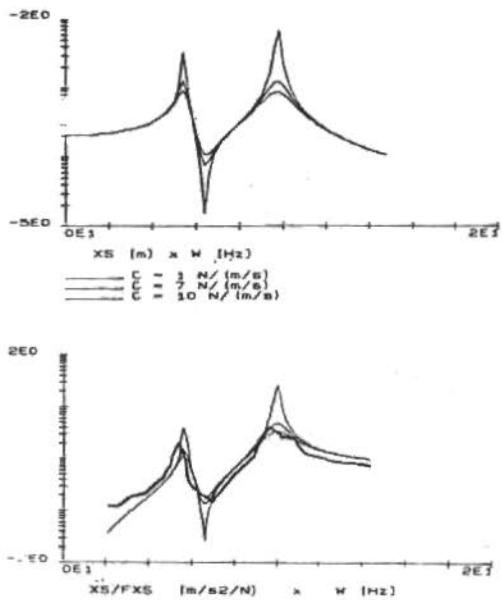

Figure 9. Calculated transfer functions (a) displacement (b) acceleration with experimental comparison

This simple method for identification is very particular to this case, but there can found similar applications in other problems. A last comparison between the eigenvalues calculated from the model and a model analysis is shown in Figure 10; the maximum error found in this case was about 17%.

1st Mode

	MEASURED	CALCULATED	
	AMPLITUDE	AMPLITUDE	PHASE (DEG)
XS	0.86	0.73	0.0
XI	1.00	1.00	0.0

2nd Mode

	MEASURED	CALCULATED	
	AMPLITUDE	AMPLITUDE	PHASE (DEG)
XS	1.00	1.00	0.0
XI	0.78	0.92	180.0

Figure 10. Model analysis results

CONCLUSION

A package of programs for the modeling and analysis of MBS is presented. The programs demostrated the power of microcomputers in this field of engineering, specially on small problems in system dynamics. The requirements, the capabilities, and the organization of a package of this kind was discussed. Some developments in fields of control engineering, non linear models and identification are yet to be done.

A small rigid rotor with flexible and damped bearings was taken as a case studied. The flexibility and damping parameters were identified from an experimental transfer function, by a simple procedure, with reasonable results.

ACKNOWLEDGEMENTS

The author wished to thank Professor Hans Ingo Weber for his extremely helpfull comments, since the very begining of our research. The author also must thank the IPEN staff for supporting this work.

REFERENCES

[1] Kortuem, W. and Schiehlen, W. – General purpose vehicle system dynamics software based on multidoby formalisms. Vehicle System Dynamics, 14 : 229-263, 1985. Swets & Zeitlinger B.V., Lisse.

[2] Kreuzer, E.; Schmoll, K.-P. and Schramm, D. – Programmpaket NEWEUL'84 Anleitung AN-10. (1984) Institut B. Fuer Mechanik, Stuttgart.

[3] Astrom, K.J. – Modelling and simulation techniques. Agard lecture series no.128, 1983).

[4] GEPROM: Relatório do Projeto DINA. (Internal Retort) Campinas, 1981.

VIBRATION CONTROL OF MAGNETICALLY SUPPORTED ROTORS

M. Frik
R. Weweries
University of Duisburg

INTRODUCTION

DUring the last years electromagnetic bearings have reached an increasing number of technical applications, e.g. for turbomolecular pumps, turbo compressors, steam turbines and rotational spindles for milling and grinding machines.

Magnetic bearings represent a suspension without mechanical contact and friction. The characteristics of the bearings, such as stiffness and damping can be chosen arbitrarily within a wide range by an appropriate design of the controller, which makes them adaptable to different dynamic requirements [1].

Furthermore, magnetic bearings can be used to control the dynamics of the suspended mechanical system during operation [2,3,4].

In this paper a magnetically suspended spindle of a milling machine is considered as an example for which vibration control during operation can be applied to improve the performance.

EQUATIONS OF MOTION

In milling machines the cutting force is the main cause of forced and self-excited vibrations which can limit the productivity and machining quality essentially. Here we are not going to describe the cutting force explicitly since it depends on a number of parameters which not all are very well known and which vary with operating conditions. Instead we shall use only its characteristic form.

It we have a constant feed of the workpiece and no oscillations of the cutter, i.e. the chip-thickness is constant, we have a time varying periodic cutting force which can be described by its constant average part and additional time varying terms. However, if oscillations of the cutter occur, we have additional time-delay terms due to the fact that the chip thickness is affected not only by the location of the cutting tooth at time t but also by the trace of the previous tooth at time t-T, with $T = 2\tau/\Omega z$, where Ω is the angular velocity of the spindle and z denotes the number of teeth of the cutter.

The time-delay terms describe the regenerative effect which can cause instability and self-excited chatter vibrations.

Since the deviations of the magnetically supported rotor from its nominal position are small, the equations of motion can be described by a linear differential equation of the form

$$M\underline{y} + P\underline{y} + Q\underline{y} = B_0\underline{u} + \underline{g}_0 + \underline{g}_1(t) + (G_0 + G_1(t))(\underline{y}(t-T) - \underline{y}(t)) + \sum_{i=1}^{\ell} W_{oi}\underline{s}_i(t) \quad (1)$$

Here $\underline{y}$ is the f-dimensional vector of the generalized coordinates, $\underline{u}$ is the r-dimensional vector of the magnetic forces, M, P, Q and B_0 are constant matrices of appropriate dimensions. The parts $\underline{g}_0$, $\underline{g}_1(t)$ and $(G_0 + G_1(t))(\underline{y}(t-T) - \underline{y}(t))$ describe the above mentioned terms caused by the cutting force. The elements of $\underline{g}_0$, $\underline{g}_1(t)$ and $\underline{G}_0$ and $\underline{G}_1(t)$ are assumed to be unkown. $W_{oi}\underline{s}_i(t)$ are harmonic excitations, e.g. caused by unbalance masses, but also harmonic parts of the cutting force may be included.

The elements of W_{oi}, i.e. amplitude and phase of these harmonic aprts are assumed to be unknown, the frequencies ω_i of

$$s_i(t) = \begin{pmatrix} \cos\omega_i t \\ \sin\omega_i t \end{pmatrix} \quad (2)$$

however, which correspond to the angular velocity of the spindle, are assumed to be known.

Introducing the state-vector $\underline{x}^T = (\underline{y}^T, \dot{\underline{y}}^T)$, the state-vector differential equation becomes

$$\dot{\underline{x}} = A\underline{x} + B\underline{u} + \underline{f}_0 + \underline{f}_1(t) + F_0\underline{s}_T + F_1(t)\underline{s}_T + \sum_{i=1}^{l} W_i\underline{s}_i \tag{3}$$

where

$$A = \begin{pmatrix} 0 & E \\ -M^{-1}Q & -M^{-1}P \end{pmatrix} ; \quad B = \begin{pmatrix} 0 \\ M^{-1}B_0 \end{pmatrix} ; \quad W_i = \begin{pmatrix} 0 \\ M^{-1}W_{0i} \end{pmatrix}$$

$$F_0 = \begin{pmatrix} 0 \\ M^{-1}G_0 \end{pmatrix} ; \quad F_1(t) = \begin{pmatrix} 0 \\ M^{-1}G_1(t) \end{pmatrix} ; \quad \underline{f}_0 = \begin{pmatrix} \underline{0} \\ M^{-1}g_0 \end{pmatrix} \tag{4}$$

$$\underline{f}_1(t) = \begin{pmatrix} \underline{0} \\ M^{-1}\underline{g}_1(t) \end{pmatrix} ; \quad \underline{s}_T = \underline{y}(t-T) - \underline{y}(t)$$

(A,B) are assumed to be controllable.

Control Schemes

Let $\underline{u}$ be composed of

$$\underline{u}(\underline{x},t) = -K\underline{x} + \underline{u}_{fo} + Z_{Fo}\underline{s} + \underline{u}_n(\underline{x}) + \sum_{i=1}^{l} Z_{Wi}\underline{s}_i \tag{5}$$

The part $-K\underline{x}$ can be designed in a common way to give the undisturbed system a desirable dynamic behavior. The terms $\underline{u}_{fo}$, $Z_{Fo}\underline{s}_T$, $Z_{Wi}\underline{s}_i$ should compensate the corresponding terms of the cutting force and the harmonic excitations, respectively.

In general not all of these compensation signals will be necessary, and we shall later on consider an example where some of these signals are omitted. However, if they are all realized we need harmonic signals, e.g. from function generators, and the generalized coordinates $\underline{y}(t-T)$, that is a part of the state-vector must be stored over the known time intervall T; $\underline{u}_n(\underline{x})$ is an additional nonlinear part of the control to be specified later on.

Inserting $\underline{u}$ into the equation of motion we obtain

$$\dot{\underline{x}} = (A - BK)\underline{x} + (\underline{f}_0 + B\underline{u}_{fo}) + (F_0 + BZ_{Fo})\underline{s}_T$$
$$+ \sum_{i=1}^{\ell} (W_i + BZ_{Wi})\underline{s}_i + \underline{f}_1(t) + F_1(t)\underline{s}_T + B\underline{u}_n(\underline{x}) \tag{6}$$

It is assumed that there exist matrices Z_{Fo}, Z_{Wi} and $\underline{u}_{fo}$ such that

$$\underline{f}_o + B\underline{u}_{fo} = \begin{pmatrix} 0 \\ --- \\ \underline{d}_f \end{pmatrix} = \begin{pmatrix} 0 \\ ----------- \\ M^{-1}(\underline{g}_o + B_o\underline{u}_{fo}) \end{pmatrix}$$

$$F_o + BZ_{Fo} = \begin{pmatrix} 0 \\ --- \\ D_F \end{pmatrix} = \begin{pmatrix} 0 \\ ----------- \\ M^{-1}(G_o + BZ_{Fo}) \end{pmatrix} \tag{7}$$

$$W_i + BZ_{Wi} = \begin{pmatrix} 0 \\ --- \\ D_{Wi} \end{pmatrix} = \begin{pmatrix} 0 \\ ----------- \\ M^{-1}(W_{oi} + B_o Z_{Wi}) \end{pmatrix}$$

become zero. This is possible if

$$\begin{aligned} \text{rank } B_o &= \text{rank}(B_o, \underline{g}_o) \\ \text{rank } B_o &= \text{rank}(B_o, G_o) \\ \text{rank } B_o &= \text{rank}(B_o, W_{oi}) \end{aligned} \tag{8}$$

In case of a rigid rotor these conditions are always satisfied since B_o has full rank.

The ramaining parts $\underline{f}_1(t) + F_1(t)\underline{s}_T$ can be interpreted as an uncertain time-varying input-signal

$$\underline{f}_1(t) + F_1(t)\underline{s}_T = C_1\underline{v}_1(t) + C_2\underline{v}_2(t) \tag{9}$$

where C_1 and C_2 are constant matrices.

It is assumed that matrices N_1 and N_2 exist such that

$$C_1 = BN_1 \quad ; \quad C_2 = BN_2 \tag{10}$$

Now let a vector $\underline{e}$ be defined as

$$\underline{e} = N_1\underline{v}_1 + N_2\underline{v}_2 \tag{11}$$

that is

$$\underline{f}_1(t) + F_1(t)\underline{s}_T = B\underline{e} \tag{12}$$

The norm of vector $\underline{e}$ is

$$||e|| \le \max_{v_1} ||N_1\underline{v}_1|| + \max_{v_2} ||N_1\underline{v}_1|| = \rho_v \tag{13}$$

If not all of the previously mentioned compensation signals are realized, the corresponding inputs may also be included in $\underline{e}$ by additional terms.

In order to derive laws for generating the compensation signals and the nonlinear control consider the Lyapunov function candidate

$$V = \underline{x}^T H \underline{x} + \underline{d}_f^T S_f \underline{d}_f + tr(D_F^T S_F D_F) + \sum_{i=1}^{\ell} tr(D_{Wi}^T S_{Wi} D_{Wi}) \tag{14}$$

where H, S_f, S_F, S_{Wi} are positive definite symmetric matrices.

The time-derivative of V is

$$\begin{aligned} \dot{V} = {} & \underline{x}^T \left[(A - BK)^T H + H(A - BK)\right] \underline{x} + 2(\underline{f}_o + B\underline{u}_{fo})^T H\underline{x} \\ & + 2\underline{s}_T (F_o + BZ_{Fo})^T H\underline{x} + 2 \sum_{i=1}^{\ell} s_i^T (W_i + BZ_{Wi})^T H\underline{x} \\ & - 2\underline{x}^T HB(\underline{u}_n + \underline{e}) + 2\underline{d}_f^T S_f \dot{\underline{d}}_f + 2tr(D_F^T S_F \dot{D}_F) \\ & + 2 \sum_{i=1}^{\ell} tr(D_{Wi}^T S_{Wi} \dot{D}_{Wi}) \end{aligned} \tag{15}$$

Since A - BK is a Hurwitz-matrix, it satisfies the Lyapunov--equation

$$(A - BK)^T H - H(A - BK) = -L \tag{16}$$

For any positive-definite symmetric matrix L, the solution of this equation is a positive definite symmetric matrix H. With the quadratic submatrices H_{ij} and the abbreviation $\underline{h}$

$$H\underline{x} = \begin{pmatrix} H_{11} & H_{12} \\ H_{21} & H_{22} \end{pmatrix} \cdot \begin{pmatrix} \underline{x}_1 \\ \underline{x}_2 \end{pmatrix} \quad ; \quad \underline{h} = H_{21}\underline{x}_1 + H_{22}\underline{x}_2 \tag{17}$$

is becomes

$$\begin{aligned}\dot{V} = & -\underline{x}^T L \underline{x} + 2\underline{d}_f^T(\underline{h} + S_f M^{-1} B_o \dot{\underline{u}}_{fo}) \\ & + 2\mathrm{tr}\left[D_F^T(\underline{hs}_T^T + S_F M^{-1} B_o \dot{Z}_{Fo})\right] + 2\underline{x}^T HB(\underline{u}_n + \underline{e}) \\ & + 2\sum_{i=1}^{\ell} \mathrm{tr}\left[D_{Wi}^T(\underline{hs}_i^T + S_{Wi} M^{-1} B_o \dot{Z}_{Wi})\right]\end{aligned} \tag{18}$$

Now we set

$$\begin{aligned}&\underline{d}_f^T(\underline{h} + S_f M^{-1} B_o \dot{\underline{u}}_{fo}) = 0 \\ &\mathrm{tr}\left[D_F^T(\underline{hs}_T^T + S_F M^{-1} B_o \dot{Z}_{Fo})\right] = 0 \\ &\mathrm{tr}\left[D_{Wi}^T(\underline{hs}_i^T + S_{Wi} M^{-1} B_o \dot{Z}_{Wi})\right] = 0\end{aligned} \tag{19}$$

which is fulfilled for

$$\begin{aligned}B_o \dot{\underline{u}}_{fo} &= -MS_f^{-1}\underline{h} \\ B_o \dot{Z}_{Fo} &= -MS_F^{-1}\underline{hs}_T^T \\ B_o \dot{Z}_{Wi} &= -MS_{Wi}^{-1}\underline{hs}_i^T\end{aligned} \tag{20}$$

These differential equations describe the laws for generating the compensation signals. Now $\dot{V}$ becomes

$$\dot{V} = -\underline{x}^T L \underline{x} + 2(B^T H \underline{x})^T (\underline{u}_n + \underline{e}) \tag{21}$$

or using (13)

$$\dot{V} \leq -\underline{x}^T L \underline{x} + 2(B^T H \underline{x})^T \left(\underline{u}_n + \frac{B^T H \underline{x}}{\|B^T H \underline{x}\|}\rho_v\right) \tag{22}$$

By an appropriate choice of $\underline{u}_n(\underline{x})$ boundedness or even asymptotic stability can be guaranteed.

a) The nonlinear control [5]

$$\underline{u}_n(\underline{x}) = -\frac{B^T H \underline{x}}{\|B^T H \underline{x}\|}\rho_v \qquad \text{for} \quad \|B^T H \underline{x}\| \neq 0$$

$$\underline{u}_n(\underline{x}) \text{ arbitrary wity } \|\underline{u}_n(\underline{x})\| \leq \rho_v \qquad \text{for} \quad \|B^T H \underline{x}\| = 0$$

leads, combined with the compensating signals (5), (20) to

$$\dot{V} \le -\underline{x}^T L \underline{x} < 0 \qquad \text{for all} \quad \underline{x} \ne \underline{0}$$

Let be $V = V_o$ for $t = t_o$, then $\underline{x}(t)$ remains within the ellipsoid $\underline{x}^T H \underline{x} = V_o$, i.e.

$$\|\underline{x}(t)\| \le \sqrt{\frac{V_o}{\lambda_{min}(H)}} \qquad \text{for all} \quad t \ge t_o$$

and $\underline{x} = 0$ is asymptotically stable.

b) A similar control scheme is obtained, if the components of $\underline{e}$ are limited by $|e_i| \le \rho_i$.

The nonlinear control

$$\begin{aligned} & u_{ni}(\underline{x}) = -\rho_n \operatorname{sgn}(\underline{b}_i^T H \underline{x}) && \text{for} \quad \underline{b}_i^T H \underline{x} \ne 0 \\ & u_{ni}(\underline{x}) \text{ arbitrary wity } |u_{ni}| \le \rho_i && \text{for} \quad \underline{b}_i^T H \underline{x} = 0 \end{aligned} \tag{24}$$

delivers

$$\dot{V} \le -\underline{x} \ L\underline{x} < 0 \qquad \text{for all} \quad \underline{x} \ne \underline{0}$$

Hence, we have the same situation as in case a).

c) The nonlinear control can also be used to avoid amplitudes of too large magnitude. If

$$\begin{aligned} & \underline{u}_n(\underline{x}) = \underline{0} && \text{for} \quad \|B^T H\underline{x}\| \le \varepsilon \\ & \underline{u}_n(\underline{x}) = -\frac{B^T H\underline{x}}{\|B^T H\underline{x}\|}\rho_v && \text{for} \quad \|B^T H\underline{x}\| > \varepsilon \end{aligned} \tag{25}$$

we obtain

for $\|B^T H\underline{x}\| > \varepsilon$: $\dot{V} = -\underline{x}^T L\underline{x}$ and

for $\|B^T H\underline{x}\| \le \varepsilon$: $\dot{V} \ne -x^T L\underline{x} + 2\varepsilon\rho_v$

which is negative for

$$\| \underline{x} \|^2 > \frac{2\varepsilon\rho_v}{\lambda_{min}(L)}$$

Example:

As a simple example the motions of a cutter are considered which is regarded as a one-degree-of-freedom-system oscillating in feed-direction only.

The equation of motion is

$$\dot{\underline{x}} = (A - BK)\underline{x} + \underline{f}_0 + \underline{f}_1(t) + (F_0 + F_1(t))(x_1(t-T) - x_1(t))$$

$$+ B[u_{f0} + z_{F0}(x_1(t-T) - x_1(t)) + u_n(\underline{x})]$$

For this one-degree-of-freedom-system u_{fo}, z_{Fo} and u_n are scalar quantities.

The cutting force can be calculated for given operating conditions such as cutter geometry, cutting speed and cutting depth etc. [6]. For the system

$$\dot{\underline{x}} = (A - BK)\underline{x} + \underline{f}_0 + F_0(x_1(t-T) - x_1(t))$$

that is for the system without compensation forces and without the time-varying parts in the cutting force, the stability limit for the onset of chatter vibrations due to the renegerative effect can be determined using the Nyquist criterion. For a given matrix A - BK, here

$$(A - BK) = \begin{pmatrix} 0 & 1 \\ -1 & -0,2 \end{pmatrix} \quad ; \quad B = \begin{pmatrix} 0 \\ 1 \end{pmatrix}$$

has been chosen, the stability limit depends upon F_0 and T. Since F_0 is proportional to the depth of cut and T is related to the rotational speed, the stability region can be described plotting depth of cut versus rotational speed. Figure 1 shows an example for a specific case.

In the following some simulation results for three operating conditions marked in Figure 1 are presented. These simulations

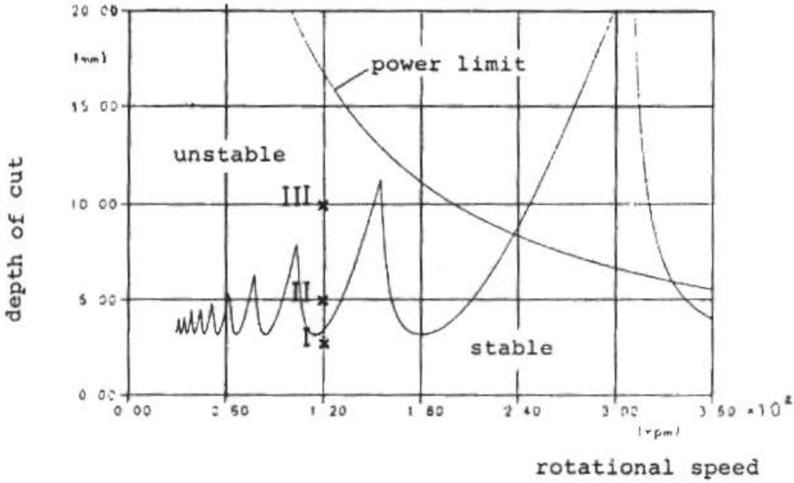

Figure 1. Stability diagramm

include all of the terms of the cutting forces, whereas different combinations of the compensation signals are applied.

For

$$L = \begin{pmatrix} 1 & 0 \\ 0 & 1 \end{pmatrix}$$

we obtain from (16) and (17)

$$h = 0.5\ x_1 + 5\ x_2$$

and from (20)

$$u_{fo} = -s_f^* h$$

$$z_{Fo} = -s_F^* h(x_1(t-T) - x_1(t))$$

where s_f^* and s_F^* are positive scalar quantities which can be chosen arbitrarily.

The nonlinear control is

$$u_n(\underline{x}) = -\rho_v \mathrm{sgn} h \qquad \text{case a) and b)}$$

$$u_n(\underline{x}) = \begin{matrix} -\rho_v \mathrm{sgn} h \\ 0 \end{matrix} \quad \text{for} \quad \begin{matrix} |h| > \varepsilon \\ |h| \leq \varepsilon \end{matrix} \qquad \text{case c)}$$

Figure 2 shows oscillations at operating points I, II, III with $u_n \equiv 0$, $z_{Fo} = 0$. The stability of I and instability of II and III are confirmed. In Figure 3 the nonlinear control of cases a) and b) is applied to operating point III without compensation of the regenerative effect. The motion $x_1(t)$ tends asymptotically towards zero. The nonlinear control has a high switching frequency, showing up also in the resulting magnetic force F_m.

For the nonlinear control of case c) and $z_{Fo} = 0$ simulation results at operating point III are given in Figure 4. Here only boundedness of the solution is obtained, but at a considerably lower switching frequency.

In Figure 5 compensation of the regenerative effect without an additional nonlinear control has been applied to point III.

The switching frequency of the nonlinear control can be reduced by hysteresis accoring to Figure 6. This nonlinear characteristic has been applied to operating point III without (Figure 7) and with (Figure 8) additional compensation of the regenerative effect. In Figure 7 the nonlinear control is needed to stabilize the system, whereas in Figure 8 it serves only to avoid large amplitudes.

CONCLUSIONS

Active magnetic bearings can be used to control the vibrations of the supported system.

It has been shown that in milling machines with magnetically supported spindles, forced and self-excited chatter vibrations can be avoided by an appropriate control of the magnetic forces, thus increasing the machining efficiency and quality. Nonlinear control schemes and compensation algorithms have been derived using the second method of Lyapunov.

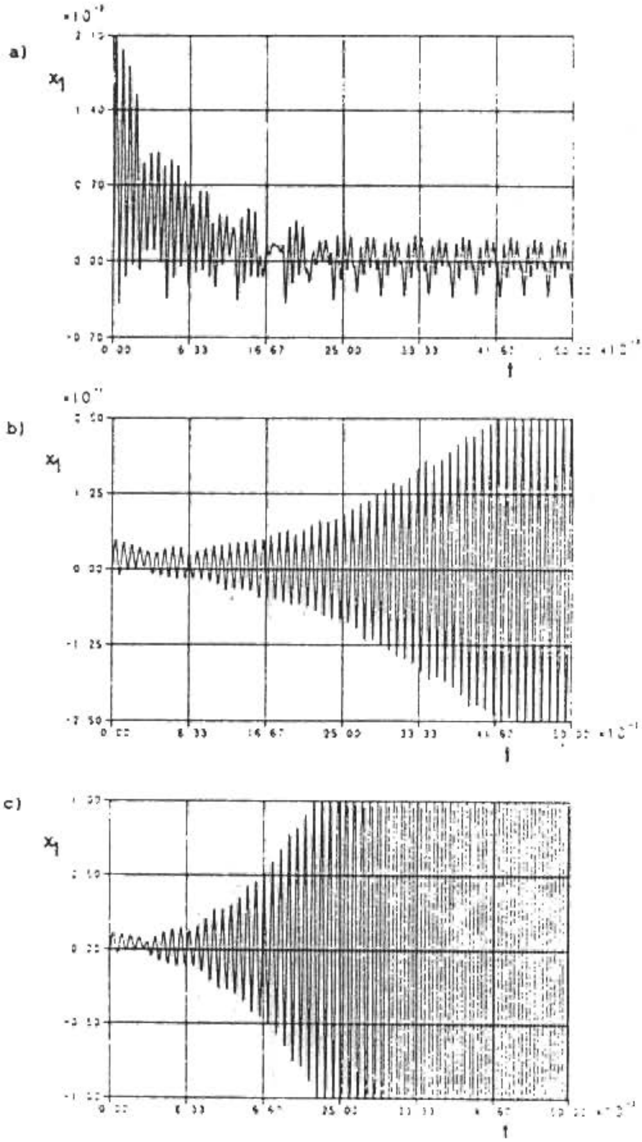

Figure 2. Vibrations $x_1(t)$ for $u_n \equiv 0$, $z_{Fo} = 0$
Operating points I, II, III

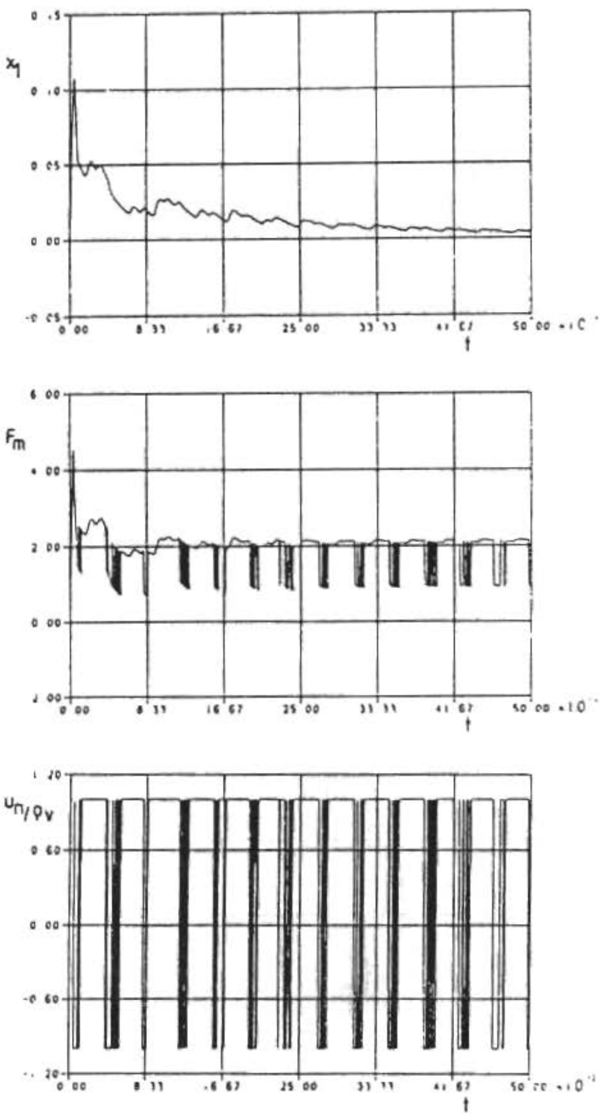

Figure 3. Operating point III, nonlinear control cases a) and b)

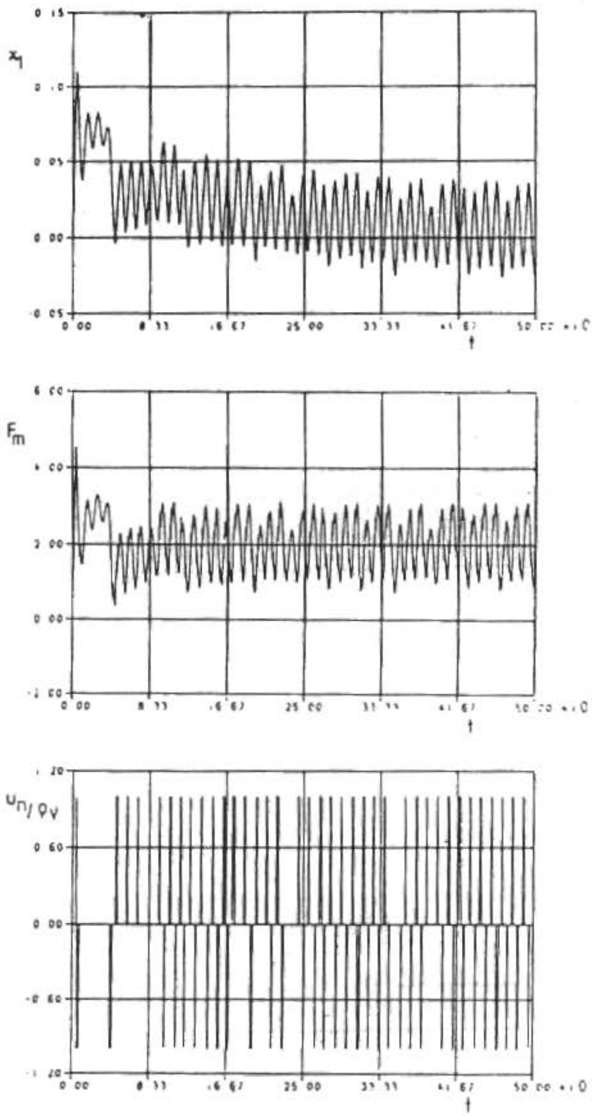

Figure 4. Operating point III, nonlinear control case c)

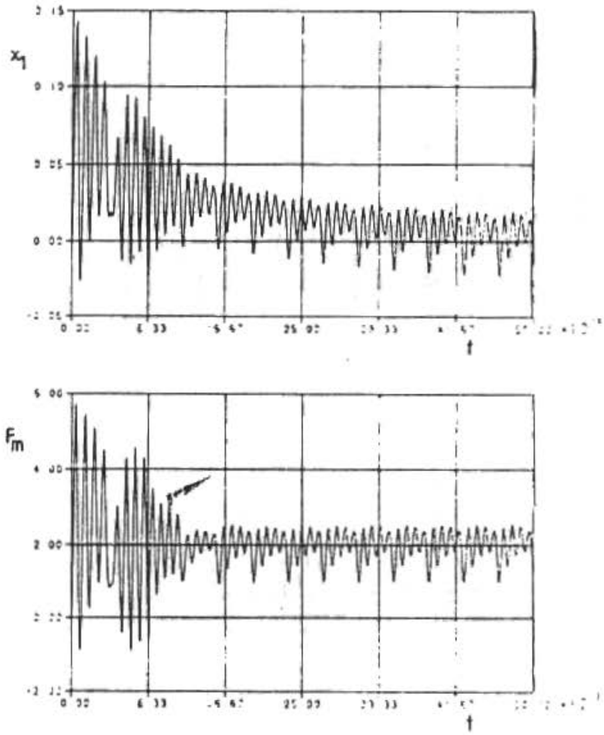

Figure 5. Operating point III, $u_n \equiv 0$

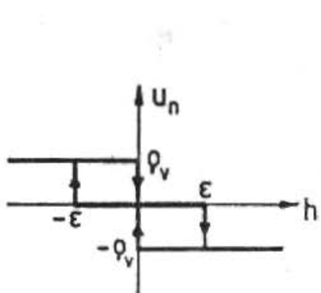

Figure 6. Nonlinear control with hysteresis

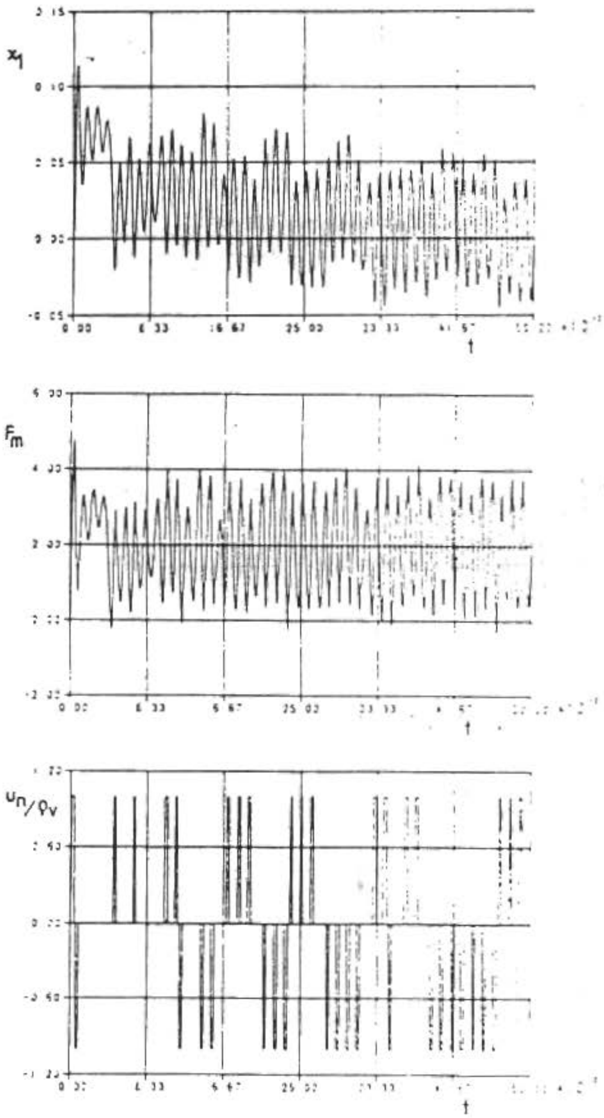

Figure 7. Operating point III, $z_{F_o} \equiv 0$, nonlinear control with hysteresis

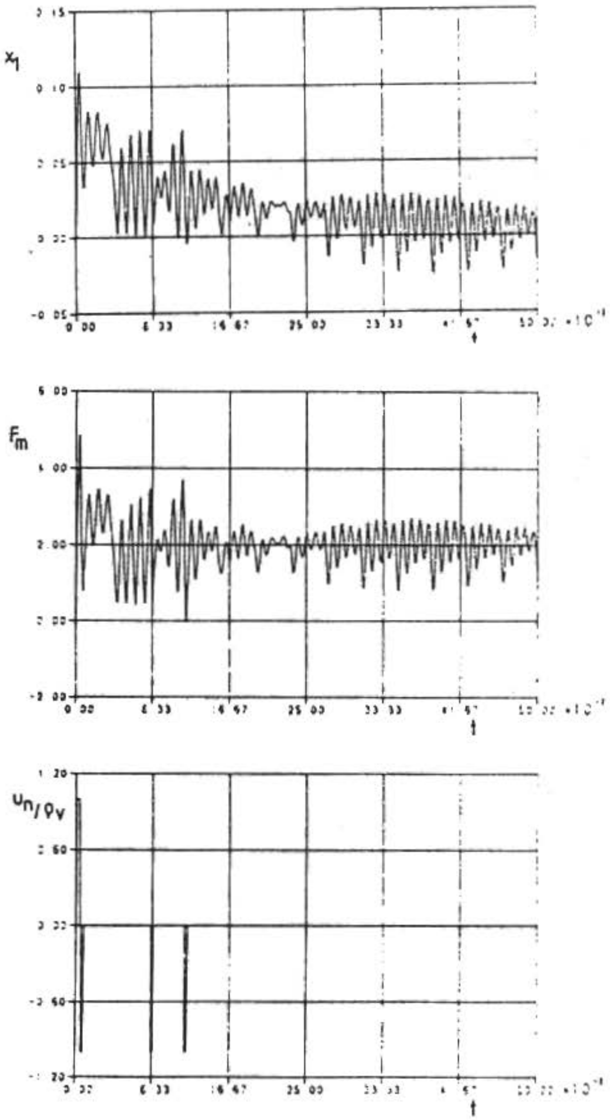

Figure 8. Operating point III, nonlinear control with hysteresis

REFERENCES

[1] Schweitzer, G. and Ulbrich, H. – Magnetic bearings - a novel type of suspension. Sec. Intern. Conf. on Vibrations in Rotating Machinery, Inst. Mech. Eng., Cambridge, 1980.

[2] Salm, J. and Schweitzer, G. – Modelling and control of a flexible rotor with magnetic bearings. Conf. on Vibr. in Rotating Machinery, Inst. Mech. Eng., York, 1984. p.553-561.

[3] Frik, M., and Blessing, R. – Rotoren in aktiven, adaptiven magnetlagern und kompensation unwuchterregter störungen. Fortschr.-Ber. VDI-Z., 8, Nr. 72, 1984, 65pp.

[4] Pietruska, W.D. and Wagner, N. – Aktive beeinflussung des schwingungs-verhaltens eines magnetisch gelagerten rotors. VDI-Bericht 456, 1982. p.129-137.

[5] Leitmann, G. – Guaranted asymptotic stability for some linear systems with bounded uncertainties. Journal of Dynamic Systems, Measurement and Control, 101 : 212-216, 1979.

[6] Weck, M. and Teipel, K. – Dynamisches verhalten spanender werkzeugmaschinen. Springer-Verlag, Berlin 1977.

A SELF-TUNING REGULATOR BASED ON POLE PLACEMENT DESIGN FOR USE IN SATELLITE ATTITUDE CONTROL

José Francisco Ribeiro
Antonio Felix Martins Neto
João Moro
Instituto de Pesquisas Espaciais – INPE/MCT
São José dos Campos, SP

ABSTRACT

The problem of controlling a three axis stabilized satellites is approached by using a self-tuning pole assigment regulator. The satellite control system is modelled as a multi input - multi output system subject to random disturbances. Ribeiro (1985) has already developed a self-tuning regulator for this same problem, considering that the system is of minimum phase and using the minimum variance criterion and the certainty-equivalence principle. In practice, some minimum phase continuous time systems are transformed into nonminimum phase sampled data systems and different response times can arise in the various loops and change with time; all these factors can impair the performance of a minimum variance self-tuning regulator. The self-tuning regulators based on pole placement try to avoid these difficulties; they are constructed in such a way to keep the closed loop system poles in values specified by designer. The certainty-equivalence principle is still used, since one admits that the system parameters are unknown, but constant, or slowly time varying. A digital simulation of a satellite is used with the following characteristics: an almost polar orbit with approximately 500km altitude and subjected to environmental disturbances (gravity gradient, aerodynamical torques, solar radiation, etc.). A set of on board sensors (Earth sensor, Sun sentor and gyrometers) is also simulated. For an analysis of performance, the results are compared with the specifications to be met by the Brazilian remote sensing satellite that will be launched in the next decade.

INTRODUCTION

The development of the microprocessor has triggered a revolution in the field of automatic control. Old results in the theory of control, that were doomed to remain simple curiosities in the text books, can now be implemented with the use of this device. Besides that, a whole variety of new techniques has appeared to take advantage of the microprocessor features. Taking into account this, it is possible nowadays to design sophisticated attitude control systems without compromising their reliability, weight and energy requirements.

The present work is a part of series of studies that have been carried or at INPE (Brazilian Institute for Space Research) with the purpose of designing a microprocessor based controller for the Brazilian Remote Sensing Satellite to be launched in the next decade. The highly nonlinear satellite dynamics is considered to be approximated by a simple multiple input - multiple output linear system with unknow parameters. A controller is then designed considering this linear system and its parameters are estimated by the usual least square method, with a variable forgetting factor to compensate the effects of changing parameters, as proposed by Fortescue et al. [1]. To check the performance of the controller, a computer simulation of the real dynamics of the satellite and of its sensors (Moro [2]) is used, and the sensor data is processed in such a way to generate torques compatible with the commercially available satellite actuators.

Ribeiro [3] has already dealt with the subject by using the approach proposed by Borison [4], Koivo [5], Bayoumi et al.[6] for a minimum phase system and a minimum covariance criterion. To deal with the problem that may arise in the case of working with a nonminimum phase system, a controller based on a pole placement design proposed by Prager and Wellstead [7] is implemented with good results.

AN OVERVIEW OF MULTIVARIABLE POLE-ASSIGNMENT SELF-TUNING REGULATORS AND THEIR APPLICATION TO SATELLITE ATTITUDE CONTROL

The whole procedure to be used throughout this work is presented in Prager and Wellstead [7]. The main steps in the design will be quickly shown.

First, it will be assumed that we are dealing with a plant which is both controllable and observable, and which is modelled by a difference equation:

$$[I + A(z^{-1})]y_t = z^{-k}B(z^{-1})u_t + [I + C(z^{-1})]c_t \quad , \tag{1}$$

where u_t and y_t are p-vectors defining the measurable system input and output, respectively, and e_t is a p-vector representing a zero--mean white noise process with covariance R. $A(z^{-1})$, $B(z^{-1})$ and $C(z^{-1})$ are polynomial matrices in the backward shift operator z^{-1}. They are of the form:

$$X(z^{-1}) = X_1 \, Z^{-1} + \ldots + X_{n_x} \, Z^{-nx} \tag{2}$$

An offline design of the regulator starts with imposing to the system a control law of the form:

$$u_t = G(z^{-1})(I + F(z^{-1}))^{-1} y_t \tag{3}$$

where

$$G(z^{-1}) = G_0 + G_1 \, z^{-1} + \ldots + G_{n_g} \, z^{-ng}$$

and

$$F(z^{-1}) = F_1 \, z^{-1} + \ldots + F_{n_f} \, z^{-nf}$$

The coefficient matrices G_i, $i = 0,1,\ldots,n_g$ and F_i $i = 1,2,\ldots,n_p$ are of dimension pxp.

The equation of the closed loop system becomes:

$$y_t = [I + F(z^{-1})][(I + P(z^{-1})^{-1}[I + C(z^{-1})]e_t \tag{4}$$

where:

$$I + P(z^{-1}) = [I + A(z^{-1})][I + F(z^{-1})] - z^{-k} \, B(z^{-1})G(z^{-1}) \quad . \tag{5}$$

Choosing $F(z^{-1})$ and $G(z^{-1})$ in such way to have:

$$I + P(z^{-1}) = [I + C(z^{-1})][I + T(z^{-1})] \tag{6}$$

the closed-loop system becomes:

$$y_t = [I + F(z^{-1})][I + T(z^{-1})]^{-1} e_t \tag{7}$$

Assuming $I + F(z^{-1})$ and $I + T(z^{-1})$ relatively prime, the poles of the system are given by $I + T(z^{-1})$ and are open to the designer's choice.

The solution to (5) and (6) requires solving the set of simultaneous linear equations:

$$(n_a+n_b+k-1)p \left\{ \begin{bmatrix} I & & (pk)\ 0 & \\ A_1 & I & \vdots & \\ \vdots & \vdots & 0 & \\ A_{n_a} & \vdots & -B_1 & \\ & \vdots & \vdots & -B_1 \\ & \vdots & -B_{n_a} & \vdots \\ & A_{n_b} & & -B_{n_b} \end{bmatrix} \right. \times \begin{bmatrix} F_1 \\ \vdots \\ F_{n_f} \\ G_o \\ \vdots \\ G_{n_g} \end{bmatrix} =$$

$$\underbrace{\qquad\qquad}_{(n_b+k-1)p} \qquad \underbrace{\qquad\qquad}_{n_a p}$$

$$= \begin{bmatrix} P_1 \\ \vdots \\ \vdots \\ P_{n_p} \end{bmatrix} - \begin{bmatrix} A_1 \\ \vdots \\ A_{n_a} \\ 0 \\ \vdots \\ 0 \end{bmatrix} \tag{8}$$

In order to generate the control u_t, it is necessary to use the fact that it is possible to find pxp matrices $\tilde{G}(z^{-1})$ and $\tilde{F}(z^{-1})$ such that:

$$\tilde{G}(z^{-1})(I + F(z^{-1})) = (I + \tilde{F}(z^{-1}))G(z^{-1}) \tag{9}$$

Using (9) in (3), it results:

$$u_t = (I + \tilde{F}(z^{-1}))^{-1} \; \tilde{G}(z^{-1}) \, y_t \tag{10}$$

and then:

$$u_t = -\tilde{F}(z^{-1}) \, u_t + \tilde{G}(z^{-1}) \, y_t \tag{11}$$

For numerically calculating the coefficient matrices $\tilde{G}_i$, $i = 0,\ldots,n_{\tilde{g}}$ and $\tilde{F}_i$, $i = 1,2,\ldots,n_{\tilde{f}}$ one needs to use the relations:

$$n_{\tilde{g}} = n_g \quad , \tag{12}$$

$$n_{\tilde{f}} = n_f \quad , \tag{13}$$

$$\tilde{G}_0 = G_0 \quad , \tag{14}$$

$$n_f + n_g \left\{ \left[\begin{array}{ccc:ccc} G_o^T & & & -I & & \\ & G_o^T & & -F_1^T & -I & \\ G_1^T & & G_o^T & \vdots & -F_1^T & \\ \vdots & G_1^T & & \vdots & \vdots & -I \\ G_{n_g}^T & \vdots & & -F_{n_f}^T & \vdots & \vdots \\ & G_{n_g}^T & & & -F_{n_f}^T & \vdots \\ & & G_{n_g} & & & -F_{n_f}^T \end{array} \right] \right. \times \begin{bmatrix} \tilde{F}_1^T \\ \tilde{F}_2^T \\ \vdots \\ \tilde{F}_{n_f}^T \\ \tilde{G}_2 \\ \vdots \\ \tilde{G}_{n_g} \end{bmatrix} =$$

$$= \begin{bmatrix} F_1^T & G_o^T \\ F_2^T & G_o^T \\ F_{n_f}^T & G_o^T \\ & 0 \\ & \vdots \\ & 0 \end{bmatrix} - \begin{bmatrix} G_1 \\ G_2 \\ \vdots \\ G_{n_g} \\ 0 \\ \vdots \\ 0 \end{bmatrix} \tag{15}$$

The offline design presupposes the knowledge of the matrix polynomials $A(z^{-1})$, $B(z^{-1})$ and $C(z^{-1})$. For the online design one should start with the model:

$$y_t = -\alpha(z^{-1})y_t + \beta(z^{-1})u_t + \varepsilon_t \tag{16}$$

where:

$$\alpha(z^{-1}) = \alpha_1 \; z^{-1} + \ldots + \alpha_{n_a} \; z^{-n_a} \tag{17}$$

$$\beta(z^{-1}) = \beta_1 \; z^{-1} + \ldots + \beta_{n_b+k} \; z^{-n_b-k} \tag{18}$$

The pxp matrix coefficients α_i, β_i are evaluated using recursive least squares. The control law is defined by equation (3), but $F(z^{-1})$ and $G(z^{-1})$ are evaluated by solving:

$$[I + \alpha(a^{-1})][I + F(z^{-1})] - \beta(z^{-1})G(z^{-1}) = I + T(z^{-1}) \tag{19}$$

As in the offline design the determinant $[I+T(z^{-1})]$ specifies the closed loop system poles. The procedure to be applied is the following:

(i) At each iteration, estimate the parameters of matrix polynomials $\alpha(z^{-1})$ and $\beta(z^{-1})$ in equations (16) using recursive least squares.

(ii) Solve equation (22) using an equation similar to equation (8).

(iii) Obtain $\tilde{F}(z^{-1})$ and $\tilde{G}(z^{-1})$ by using an equation similar to (15) and get an expression of the control law as in (10).

(iv) Calculate u_t from the law obtained in step (iii).

APPLICATION OF SELF-TUNING REGULATOR THEORY TO SATELLITE CONTROL

The highly nonlinear satellite dynamics will be approximated by the following linear model:

$$y(t) + A_1 \; y(t-1) + A_2 \; y(t-2) = B_1 \; u(t-2) + B_2 \; u(t-3) + e_t \quad , \tag{20}$$

where:

$y(t)$ - 3 dimension observation vector,
$u(t)$ - 3 dimension torque vector,
$A_i, B_i, i = 1,2$ - 3x3 matrices.

The control law to be implemented will be:

$$u(t) = (G_0 + G_1 z^{-1})(I + F_1 z^{-1} + F_2 z^{-2})^{-1}\ y(t) \tag{21}$$

The matrix $T(z^{-1})$ to be the designers choice is of the following form:

$$I + T(z^{-1}) = T_1 z^{-1} + T_2 z^{-2} + T_3 z^{-3} + T_4 z^{-4} \tag{22}$$

The formulas for calculating $F(z^{-1})$, $\tilde{F}(z^{-1})$ and $\tilde{G}(z^{-1})$ are respectively:

$$\begin{bmatrix} I & 0 & 0 & 0 \\ A_1 & I & -B_1 & 0 \\ A_2 & A_1 & -B_2 & -B_1 \\ 0 & A_2 & 0 & -B_2 \end{bmatrix} \begin{bmatrix} F_1 \\ F_2 \\ G_0 \\ G_1 \end{bmatrix} \begin{bmatrix} T_1 \\ T_2 \\ T_3 \\ T_4 \end{bmatrix} - \begin{bmatrix} A_1 \\ A_2 \\ 0 \\ 0 \end{bmatrix} \tag{23}$$

$$\tilde{G}_0 = G_0 \quad , \tag{24}$$

$$\begin{bmatrix} G_0^T & 0 & -I \\ G_1^T & G_0^T & -F_1^T \\ 0 & G_1^T & -F_2^T \end{bmatrix} \begin{bmatrix} \tilde{F}_1^T \\ \tilde{F}_2^T \\ \tilde{G}_1^T \end{bmatrix} = \begin{bmatrix} F_1^T & G_0^T & -G_1^T \\ F_2^T & G_0^T & \\ & 0 & \end{bmatrix} \tag{25}$$

For the online identification of A_i, B_i, $i = 1,2$

$x(t-1) \triangleq [-y^T(t-1),\ -y^T(t-2),\ u^T(t-2),\ u^T(t-3)]$

$\Theta(t-1) \triangleq [A_1 \mid A_2 \mid B_1 \mid B_2]^T \triangleq [\Theta_1, \Theta_2, \Theta_3]$

are defined.

Using this notation, the equation to be used in the recursive least square method becomes:

$$y_i(t) = x(t-1)\ \Theta_i(t-1) + \varepsilon_i(t) \quad , \qquad i = 1,2,3 \quad . \tag{26}$$

The recursive estimate $\hat{\theta}_i$ of the parameters θ_i is calculated at each step by applying the formulas:

$$\hat{\theta}_i(t) = \hat{\theta}_i(t-1) + K(t-1)[y_i(t) - x(t-1)\ \hat{\theta}_i(t-1)]\ , \quad i = 1,2,3$$

$$K(t-1) = \frac{P(t-1)\ x^T(t-1)}{1 + x(t-1)\ P(t-1)\ x^T(t-1)}$$

$$P(t) = \frac{1}{\alpha}\left\{P(t-1) - K(t-1)[1 + x(t-1)\ P(t-1)\ x^T(t-1)]K^T(t-1)\right\}$$

where:

α is a forgetting factor that is obtained by using a method presented by Fortescue et al.[1].

For defining the requirements of be met by the control system, the following references systems should be defined (see Figure 1):

i) Orbital System ($O\bar{x}\bar{y}\bar{z}$) - origin in the satellite center of mass, y-axis perpendicular to the orbital plane, z-axis pointing outwards from the orbital ellipse and x-axis complementing the right -handed system.

ii) Mobile System (Mxyz) - origin in the satellite center of mass and axis fixed in the satellite body.

iii) Inertial Reference System (Ixyz) - an inertial reference system translated to the satellite center of mass.

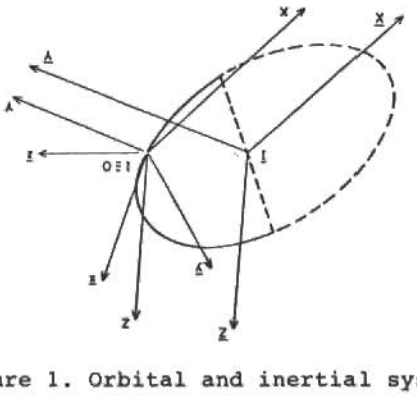

Figure 1. Orbital and inertial systems

The goal of the control system is to coincide the orbital system with the mobile system in steady state, what would imply that the satellite, way axis is aligned with the Earth Center and, consequently, the on board multispectral camera is correctly positioned. The requirements at steady state should be:

a) the angles between the x-axis (DELX), the y-axis (DELY) and the z-axis (DELZ) of the mobile system and the corresponding axis of the orbital system can not be more than 0.5^{o}.

b) the angular velocities in the mobile system should be such that:
$- 0.0065^{o}/s < W_x < 0.0065^{o}/s$,
$- 0.0065^{o}/s < W_y < 0.0065^{o}/s$,
$- 0.01^{o}/s < W_z < 0.01^{o}/s$.

The output y(t) is constructed making use of the on board sensor observations (Sun sensor, Earth sensor and gyrometers) and the Sun and Earth position data. With this piece of information the rotation matrix between the orbital system and the mobile system can be determined.

The mobile system should coincide with the orbital system within a predetermined error, that is to say, the rotation matrix should be as much as possible equal to the identity matrix.

The output y(t) is defined as:

$$y(t) = K_1 \phi E(t) + K_2 (w(t) - w_r(t))$$

where $y(t) \epsilon R^3$ is the output; K_1, K_2 are 3x3 diagonal matrices with positive elements; $E(t)$ and ϕ are respectively the rotation versor and the rotation angle associated with the rotation matrix; $w(t) - w_r(t)$ is the angular velocity between the mobile system and the orbital system measured in the mobile system. Ribeiro [3] has shown that if in steady state the output y(t) is zero, then the mobile system agrees with the orbital system.

SIMULATION RESULTS

For simulating the satellite dynamics and the sensor data, the work developed by Moro [2] was used utilizing the satellite TD-1A parameters (Tilgner [8]). Its moments of inertia are respectively $I_{xx} = 207$ kgm², $I_{yy} = 225$ kgm² and $I_{zz} =$ kgm². Gravity gradient, aerodynamical drag and solar radiation were the environmental torques considered, following the model proposed by Carrara [10]. The constant K_1 and K_2 used in the output process y_t were chosen respectively 1 and 20.

To verify the controller performance it was considered that the satellite was in the process of attitude acquisition. Within the imposed requirements, the control system should be able to acquire the correct attitude and keep it within bounds during steady state. With this purpose, the angles DELX, DELY and DELZ should be considered to have deviation in modulus of less than 15° from the desired steady state attitude with $\|w_x\|$, $\|w_y\|$ and $\|w_z\|$ equal to 2°/s in the worst case. Taking into account the experience already achieved by other works (Ribeiro [3] and Ribeiro et al.[9], it a sampling interval of 1 second and a matrix $T(z^{-1})$ with coefficient matrices:

$$T_1 = -0.5I \quad T_2 = T_3 = T_4 = \phi$$

were chosen:

The initial parameters to be used in equation (10) were:

$$A_1 = I \quad , \quad A_2 = I \quad , \quad B_1 = I \quad , \quad B_2 = I$$

The initial covariance matrix for the parameters was fixed in 100 I, and $\Sigma_0 = 0.05$ was applied in dealing with the variable forgeting factor.

Figure 2 to 7 show the behavior of DELX, DELY, DELZ, w_x, w_y, w_z, respectively. For the sake of clarification, each figure is presented with two different scales for showing the overall response and the response near equilibrium at steady state. It can be verified that the proposed controller keeps the angular deviations and the angular velocities within the proposed bounds and reaches steady state in a compatible time (less than 500 sec). The rotation angle is also shown (Figure 8).

The variable forgetting factor evolution in time is shown in Figure 9.

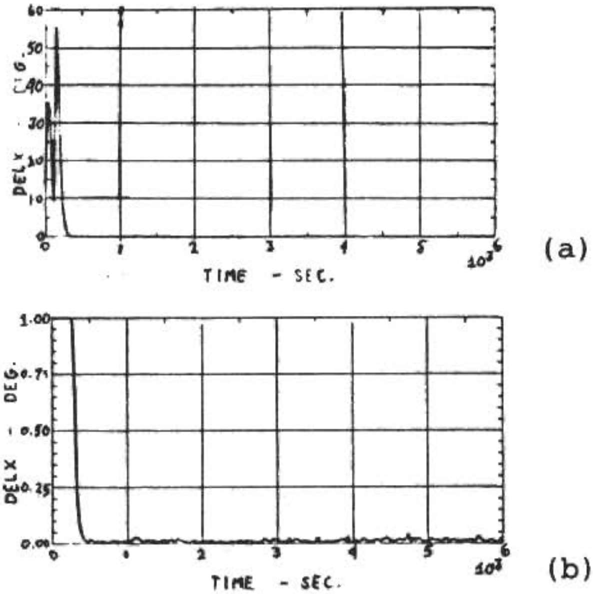

Figure 2. DELX

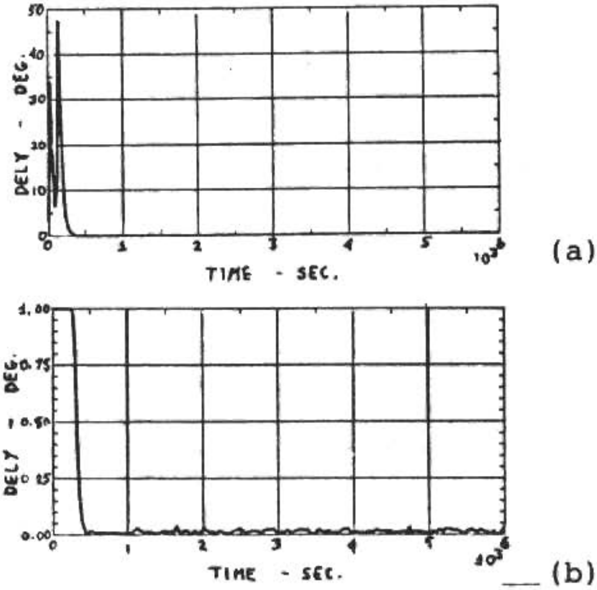

Figure 3. DELY

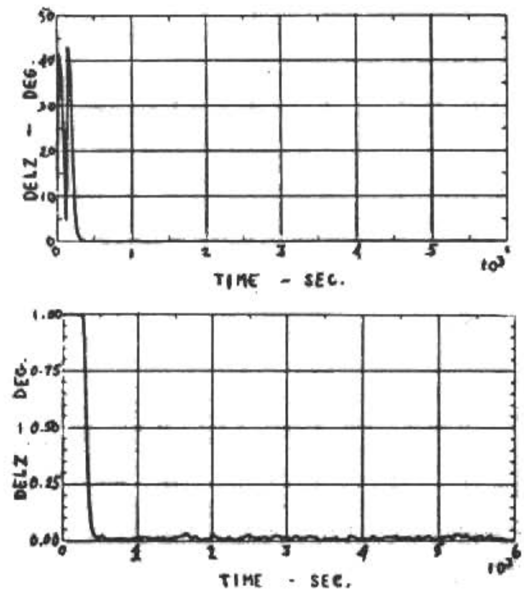

(a)

(b)

Figure 4. BELZ

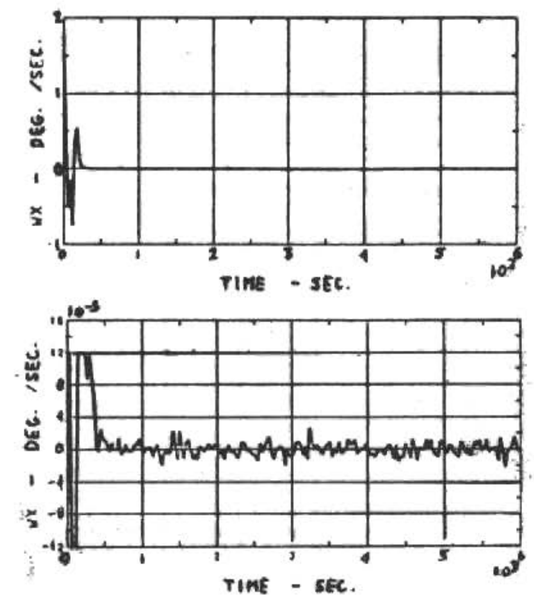

(a)

(b)

Figure 5. W_x

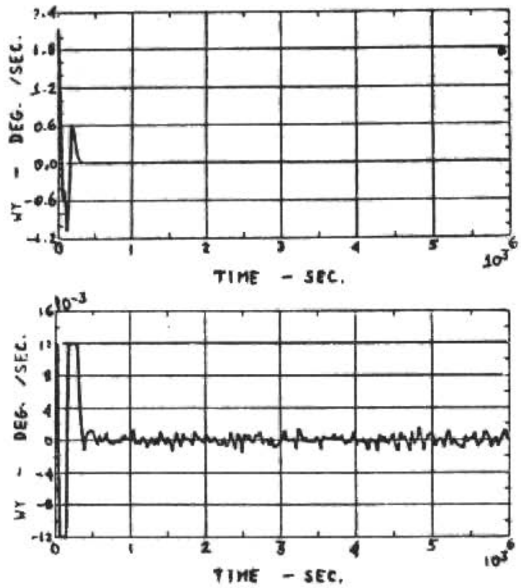

(a)

(b)

Figure 6. W_y

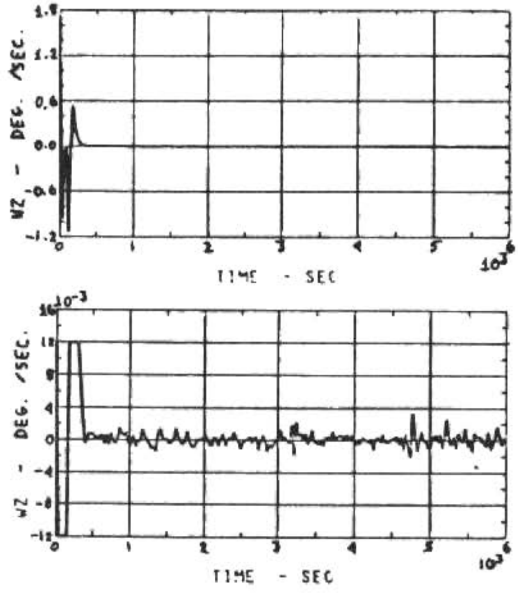

(a)

(b)

Figure 7. W_z

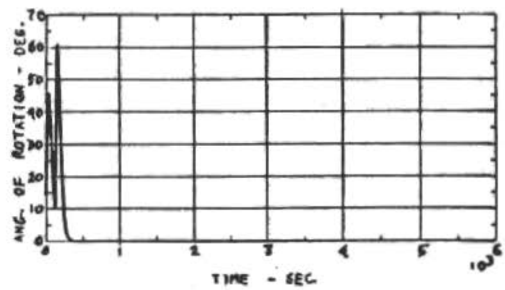

Figure 8. Angle of rotation

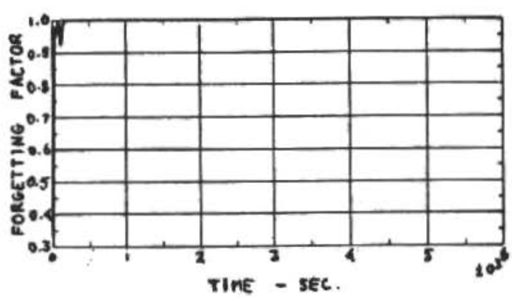

Figure 9. Forgetting factor

Since there is a limitation in the amount of torques that a momentum exchange device can supply, it is important to check whether the controller generates outputs within bounds. It was considered that the satellite will be supplied with a maximum torque capability of 2 N.m per axis. Figure 10.a and b shows that this limit is not exceeded by the designed controller.

TO complete the analysis the actual output (Figure 10) is shown. It can be seen that, after the system has reached steady state, the output consists of noise coming from the instruments for measuring the attitude and the angular velocity.

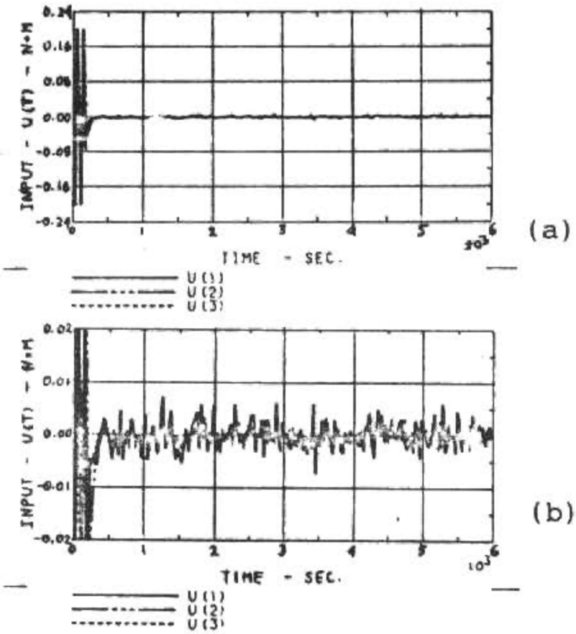

Figure 10. Inputs

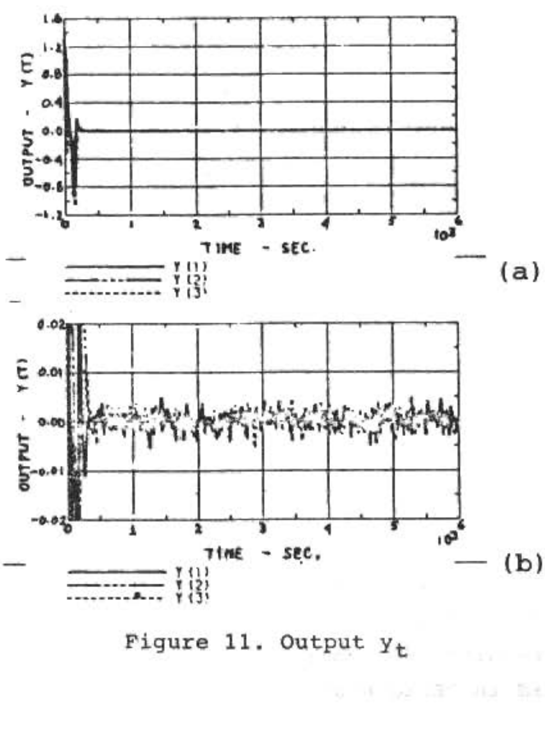

Figure 11. Output y_t

[10] Carrara, V. — Modelagem das forças e torques atuantes nos satélites. Dissertação de Mestrado em Ciências Espaciais, São José dos Campos, INPE, 1982 (INPE-2454-TDL/094).

CONCLUSION

The proposed method of dealing with the attitude control has shown a good effectiveness that allows the fulfilment of the simulated mission requirements. The great versatility, the small torques that are obtained, the fast velocity of convergence are very good features observed in the tests.

If this controller is compared with the one already proposed by Ribeiro et al.[9], it can be verified that a greater overshoot is obtained for all variables. This is the penalty for not using an optimal procedure. But this disadvantage can be compensated by the fact that the risk of dealing with monminimum phase systems is avoided.

REFERENCES

[1] Fortescue, T.R.; Kershenbaum, L.S. and Ydstie, B.E. - Implementation of self-tuning regulators with variable forgetting factors. Automática, 17 : 6, 1981.

[2] Moro, J. - Modelagem, análise e síntese preliminar de um sistema de controle de atitude em três eixos para satélites artificiais. Tese de Doutorado em Engenharia, SP, USP, 1983.

[3] Ribeiro, J.F. - O Uso de controle auto-sintonizado num sistema de controle de atitude ativo em três eixos de um satélite artificial de sensoriamento terrestre. Dissertação de Mestrado em Ciências Espaciais, São José dos Campos, INPE, 1985.

[4] Borison, U. - Self-tuning regulators for a class of multivariable systems. Automática, 15 : 209-215, 1979.

[5] Koivo, H.N. - A multivariable self-tuning controller. Automática, 16 : 351-366, 1980.

[6] Bayoumi, M.N.; Wong, K.Y. and El-Bagoury, M.A. - Self-tuning regulator for multivariable systems. Automática, 17 (4) : : 572-592, 1981.

[7] Prager, D.L. and Wellstead, P.E. - Multivariable pole--assignment self-tuning regulators. IEE Proceedings, vol. 128, Pt.D, no.1, 9-18, 1980.

[8] Tilgner, B. - The TD-1A satellite. ELDO/ESRO Scientific and Technical Review, 3 (4) : 567-609, Oct/Dec. 1971.

[9] Ribeiro, J.F.; Moro, J. and Martins Neto, A.F. - Artificial satellite attitude control using a self-tuning controller. Presented in TELECON'85.

SEMINAR IN MACHINERY NOISE AND DIAGNOSTICS

This six-day seminar, taught by Professor Richard H. Lyon, of M.I.T., will be offered the week of 10-15 August 1987, in Cambridge, Massachusetts. The seminar teaches the design principles for making machines operate more quietly, and the use of vibration and acoustical signals to determine faults in operating machines. Sources of noise and vibration in machines, the transmission and radiation of acoustical energy by the machine , and signal processing methods for fault signature recovery will be covered in the lectures and demonstrations. The text for the course is Professor Lyon's new book, Machinery Noise and Diagnostics.

For further information contact:

Prof. R.H. Lyon, Rm. 3-366
Mass. Inst. of Technology
Cambridge, Mass. 02139 - USA